

Report 9, 1990

**LUMPED AND DISTRIBUTED PARAMETER MODELS OF
THE MOSFELLSSVEIT GEOTHERMAL FIELD, SW-ICELAND**

Mica Martinovic,
UNU Geothermal Training Programme,
Orkustofnun - National Energy Authority,
Grensasvegur 9,
108 Reykjavik,
ICELAND

Permanent address:
Faculty of mining and geology,
Hydrogeology,
Djusina 7,
Beograd,
YUGOSLAVIA

ABSTRACT

The main part of this report is addressed to the groundwater flow modelling of the Mosfellssveit geothermal field. First, a simple lumped model of the field was made in order to match measured and calculated pressure response with the present production rates on a monthly basis from 1971 to 1989. After calibration of the model, future water level changes with different monthly and yearly production rates were estimated in order to predict pressure response of the field until the year 2000.

The second part consisted of making a distributed groundwater flow model of the field in order to determine the distribution of the main hydraulic parameters.

The main problem in the behaviour of the field is the constant lowering of the water level due to high production. During exploitation of the field, no significant changes in temperature or chemical content have been observed.

TABLE OF CONTENTS

	Page
ABSTRACT	3
TABLE OF CONTENTS	4
LIST OF FIGURES	5
LIST OF TABLES	5
1. INTRODUCTION	6
2. GENERAL FEATURES OF THE MOSFELLSSVEIT GEOTHERMAL FIELD	7
2.1 Locality	7
2.2 Geology	7
2.3 Hydrogeology	10
2.4 Geophysics	12
2.5 Temperature	13
2.6 Production history	13
2.7 Utilization	17
3. LUMPED PARAMETER MODEL	19
3.1 General overview	19
3.2 Theoretical basis	19
3.3 Results of lumped parameter model	23
3.4 Future prediction of the water level	24
3.4.1 Future prediction, case 1	25
3.4.2 Future prediction, case 2	25
3.4.3 Future prediction, case 3	28
4. DISTRIBUTED PARAMETER MODEL	30
4.1 General overview	30
4.2 Theoretical basis with emphasis on the AQUA programme	30
4.2.1 Flow model	30
4.2.2 Mass transport model	32
4.2.3 Heat transport model	33
4.3 Basis of the model	34
4.3.1 Basic assumptions	34
4.3.2 Establishing the boundary conditions	34
4.3.3 Initial parameter values	34
4.4 Results of the distributed parameter model	35
4.4.1 Transmissivity	35
4.4.2 Storage coefficient	37
4.4.3 Anisotropy	39
4.4.4 Drawdown	39
5. CONCLUSIONS AND RECOMMENDATIONS	43
ACKNOWLEDGEMENTS	44

	Page
NOMENCLATURE	45
REFERENCES	47

LIST OF FIGURES

1. Geological situation of the Mosfellssveit geothermal field	7
2. Simplified geological section of the Reykir and Reykjahlid wells	8
3. Location of boreholes in Reykir and Reykjahlid	9
4. Resistivity map of Reykjavik and vicinity	10
5. Gravity map of Reykjavik and vicinity	11
6. Temperature profiles of wells in Reykir	11
7. Temperature profiles of wells in Reykjahlid	11
8. Map of the maximum temperatures in Mosfellssveit geothermal field	12
9. Reykir: annual production (GJ), 1971-1989	14
10. Reykjahlid: annual production (GJ), 1971-1989	15
11. Mosfellssveit: annual production (GJ), 1971-1989	16
12. Location map of the Reykjavik low temperature fields	17
13. Simplified lumped parameter model	20
14. Unit response function	24
15. Measured and calculated drawdown for the Mosfellssveit geothermal field	25
16. Mosfellssveit, monthly production rates 1989	26
17. Future prediction, case 1	26
18. Mosfellssveit, monthly production used for case 2	27
19. Future prediction, case 2	27
20. Future prediction, case 3	29
21. Boundary conditions of the model	35
22. Map of transmissivities	36
23. Map of storage coefficients	36
24. Changes in storage coefficient during exploitation	37
25. Map of anisotropy angles	38
26. Anisotropy $\sqrt{T_{yy}/T_{xx}}$ map	38
27. Measured and calculated drawdown, Reykir	39
28. Measured and calculated drawdown, Reykjahlid	40
29. Measured and calculated drawdown, Stardalur	40
30. Calculated drawdown for Mosfellssveit geothermal field, year 1990	41
31. Calculated drawdown for Mosfellssveit geothermal field, year 2000	42

LIST OF TABLES

1. Occurrence of aquifers in different rock types of 29 drill holes	10
2. Reykir: monthly production (GJ), 1971-1989	14
3. Reykjahlid: monthly production (GJ), 1971-1989	15
4. Mosfellssveit: monthly production, (GJ), 1971-1989	16
5. Future prediction: drawdown with different production rates, 1990-2000	28

1. INTRODUCTION

The author of this work had the privilege to participate in the six months' training course of the UNU Geothermal Training Programme at the National Energy Authority in Reykjavik, Iceland in the summer of 1990. The programme started with a 5 week introductory course about all relevant geological aspects connected with geothermal energy. For the next 4 weeks, the author received specialized lectures and practical training in borehole geophysics and reservoir engineering. A field excursion and seminars were organized from 10.07. to 18.07.1990. During our field trip we visited low and high temperature geothermal fields in southern and northern Iceland. Practical field work in well testing in the Reykir low temperature field and in the Krafla high temperature field took place for one week. The final 8 weeks of the training course concentrated on the theoretical basis of lumped and distributed groundwater flow and transport modelling with practical applications on the modelling of the Mosfellssveit geothermal field.

2. GENERAL FEATURES OF THE MOSFELLSSVEIT GEOTHERMAL FIELD

2.1 Locality

The Mosfellssveit low temperature geothermal field is located in southwest Iceland, 15-20 km from the city of Reykjavik and has been the principal source of thermal water for the Reykjavik Municipal District Heating Service since 1944. The Mosfellssveit field is divided into two sub-areas, Reykir to the south and Reykjahlid to the north. The distance between them is about 2-3 km. The elevation of both fields is 40-80 m above mean sea level (amsl). The sub-areas are separated by the low mountains Helgafell, Aesustadafell and Reykjafell, which rise to an elevation of 200 to 250 m amsl.

2.2 Geology

Geologically, the field is located on the western flank of the neo-volcanic zone in southwest Iceland between the extinct central volcanoes Kjalarnes and Stardalur, but closer to the southwestern margin of the Stardalur volcano (Figure 1). There are signs of ten glaciations in the volcanic succession. The rate of volcanic eruption was much higher in the central volcanoes than

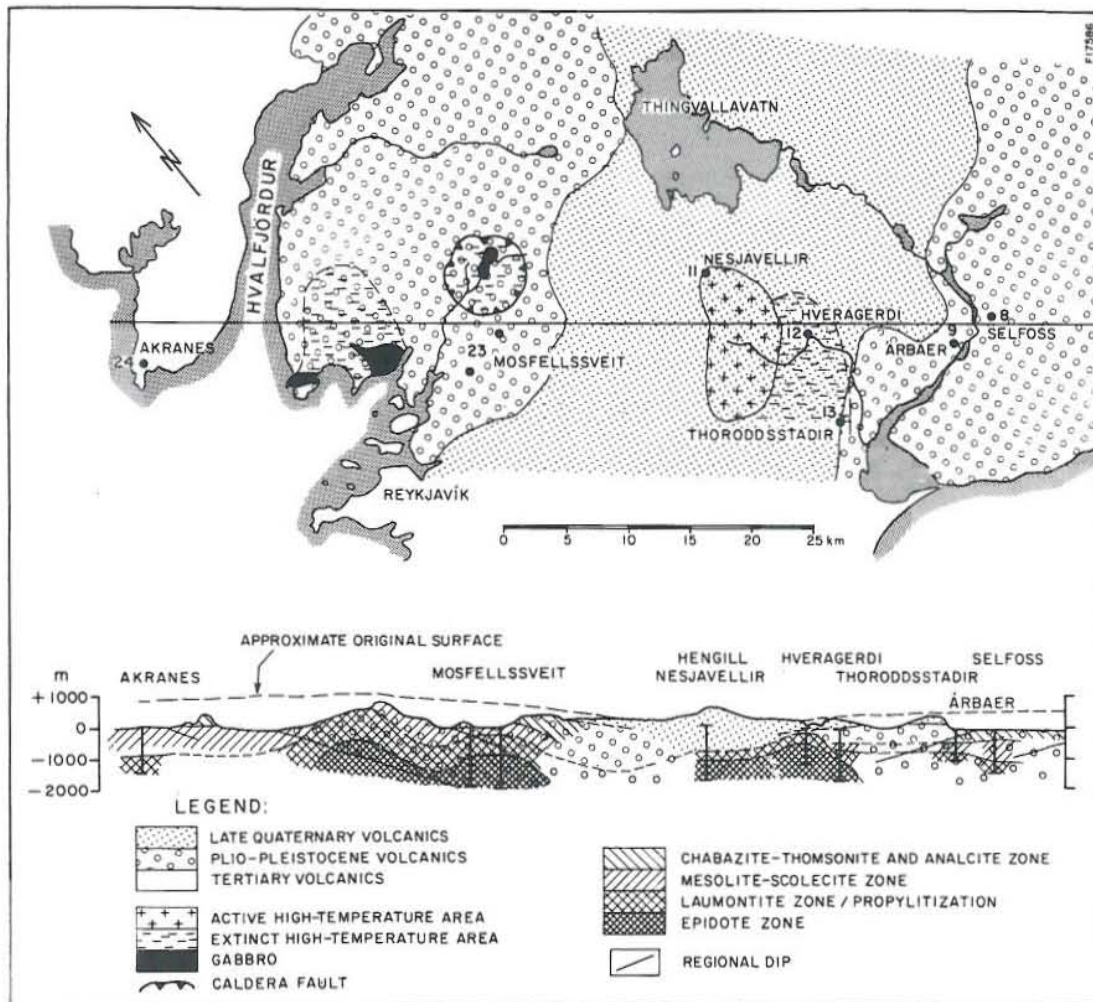


FIGURE 1: Geological situation of the Mosfellssveit geothermal field (Palmason et al. 1978)

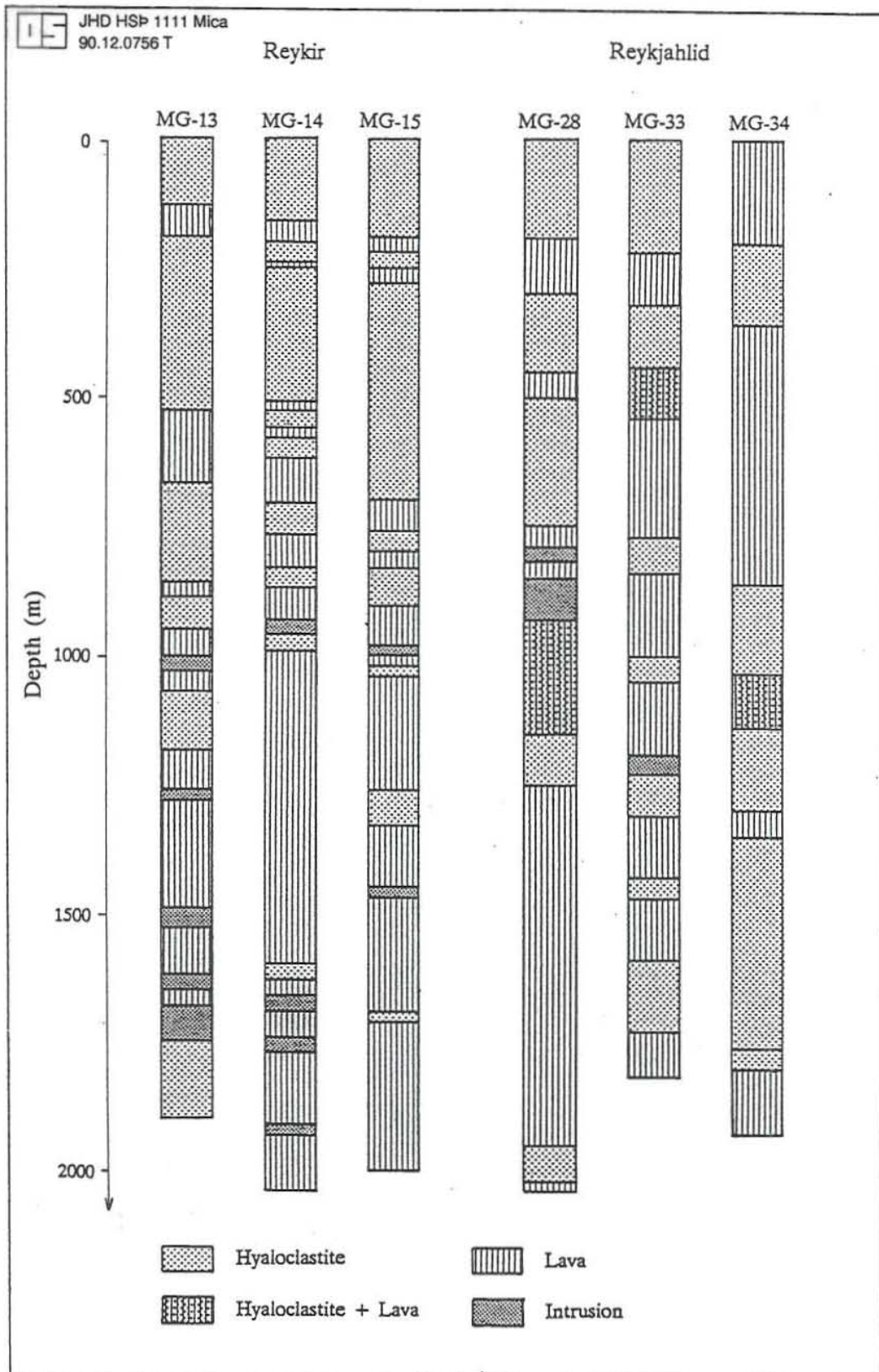


FIGURE 2: Simplified geological section of the wells in Reykir and Reykjahlid

parts of the volcanic zone in other parts of the volcanic zone of the time. This resulted in exceptionally thick accumulations of hyaloclastites in the vicinity of the volcanoes during glacial periods (Fridleifsson, 1973). The age of the rocks is in the range of 2.8 to 1.8 m.y. Plio-Pleistocene strata reaches to a depth of at least 2000 m.

Stratigraphically, the cross-section through the area is characterized by sequences of subaerial lava flows intercalated by volcanic hyaloclastites and morainic horizons at intervals corresponding to glacial periods. Hyaloclastites are dominant to about 1000 m depth. Dykes are rare in the uppermost 1000 m, but their number tends to increase with depth. The ratio of hyaloclastites to subaerial lavas in the strata is variable within the Mosfellssveit geothermal field; in 29 drillholes 800 to 2043 m deep, the volume percentage of hyaloclastites ranges from 30 to 60%. Consider a 2 km deep hole with approximately 1000 m of lavas, 900 m of hyaloclastites, and 100 m of intrusions, but perhaps only 40 to 50 narrow contacts (aggregate thickness to the order of 100 m) between lavas and hyaloclastites. The chances of aquifers occurring in lavas alone are perhaps tenfold to those of contacts between the formations. (Tomasson et al., 1975).

Simplified lithological cross-sections of some typical profiles from the wells in Reykir and Reykjahlid geothermal fields are shown in Figure 2. Locations of the same wells are shown in Figure 3.

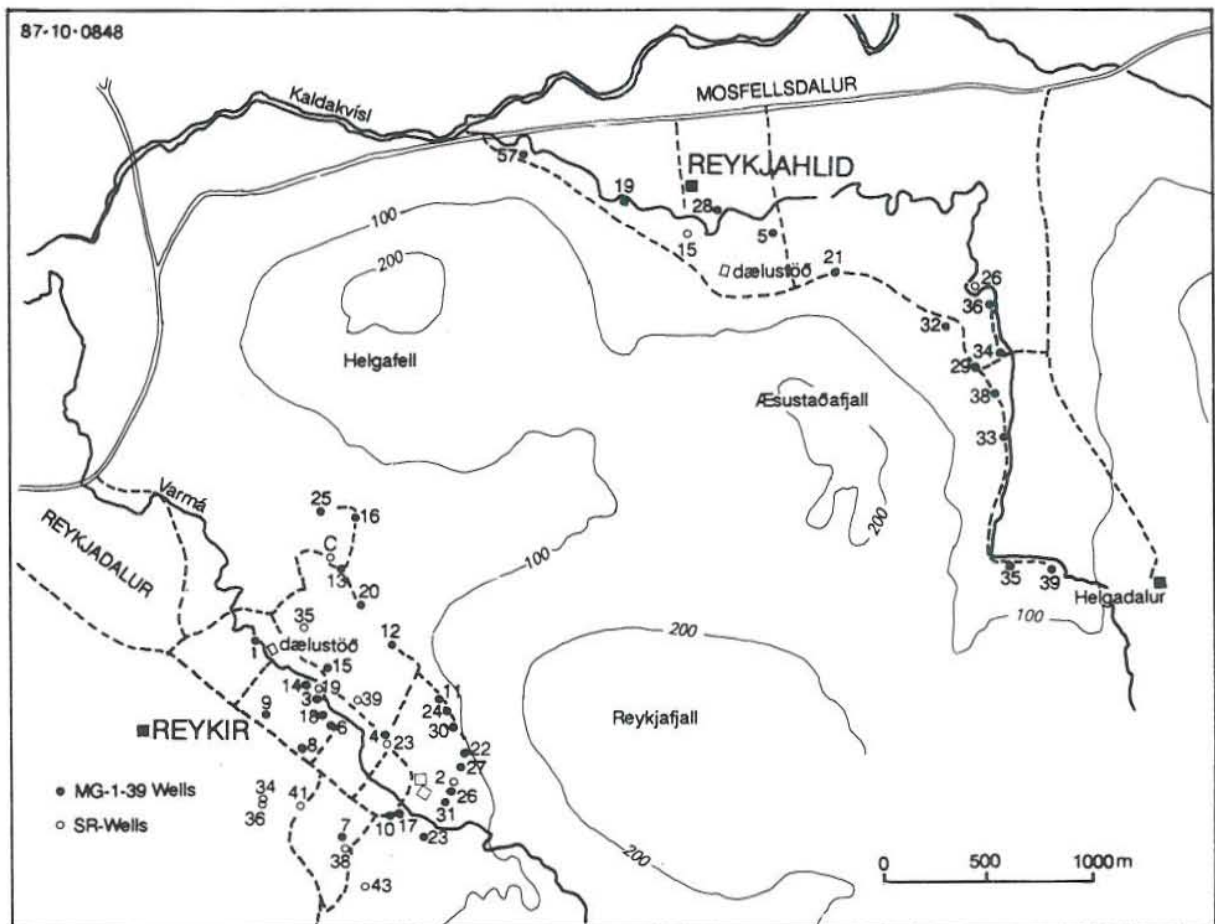


FIGURE 3: Location of the boreholes in Reykir and Reykjahlid

2.3 Hydrogeology

Aquifers are irregularly distributed through the geological section but are common at the contact between lava flows, hyaloclastites and dolerite intrusions. The average porosity of subglacial volcanics is approximately twice that of subaerial lavas (Fridleifsson, 1975).

The hyaloclastite ridges can be looked on as high-porosity channels separated by relatively low porosity lavas in the Quaternary strata. Table 1 shows the occurrence of aquifers in the different rock types in the first 29 drillholes in the area. From the table, it is obvious that if we have a higher number of contacts between lavas and hyaloclastites, there is a higher number of aquifers (Tomasson et al., 1975).

TABLE 1: Occurrence of aquifers in different rock types of 29 drill holes (Tomasson et al., 1975)

Rock type	Aquifers/circulation loss			Total number
	= 2 l/s	2-20 l/s	> 20 l/s	
Lavas	44	27	2	73
Hyaloclastites*	29	12	4	45
Dolerites		1	1	2
Lavas and hyaloclastites*	53	38	20	111
Lavas and dolerites	13	1	3	17
Hyaloclastites* and dolerites	5	2	1	8

* included in this group are reworked hyaloclastites and detrital beds

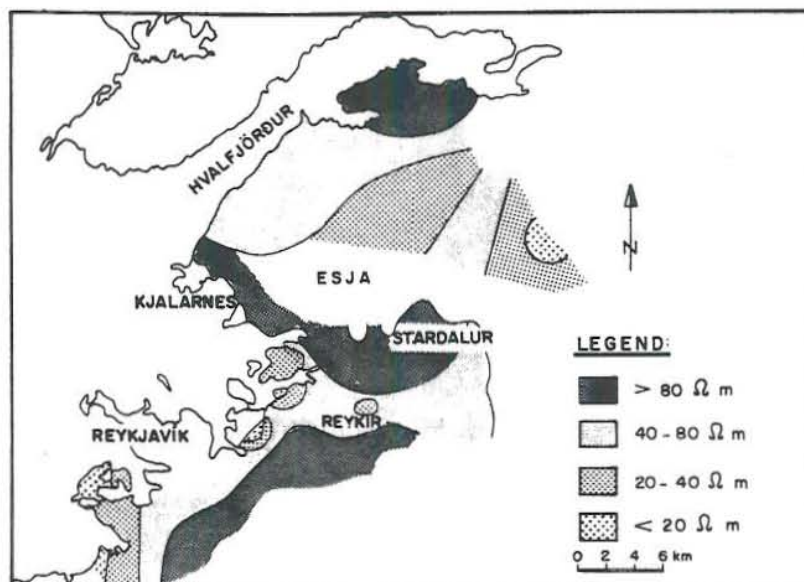


FIGURE 4: Resistivity map of Reykjavik and vicinity (Tomasson et al., 1975)

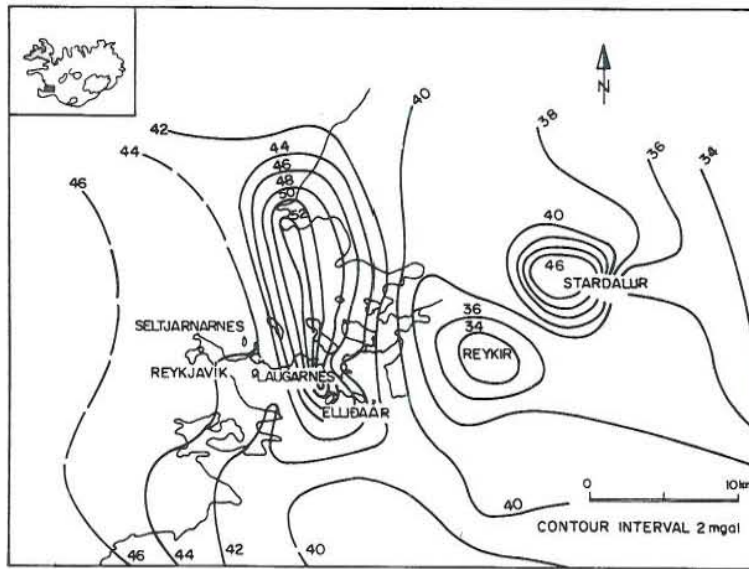


FIGURE 5: Gravity map of Reykjavik and vicinity (Einarsson, 1954)

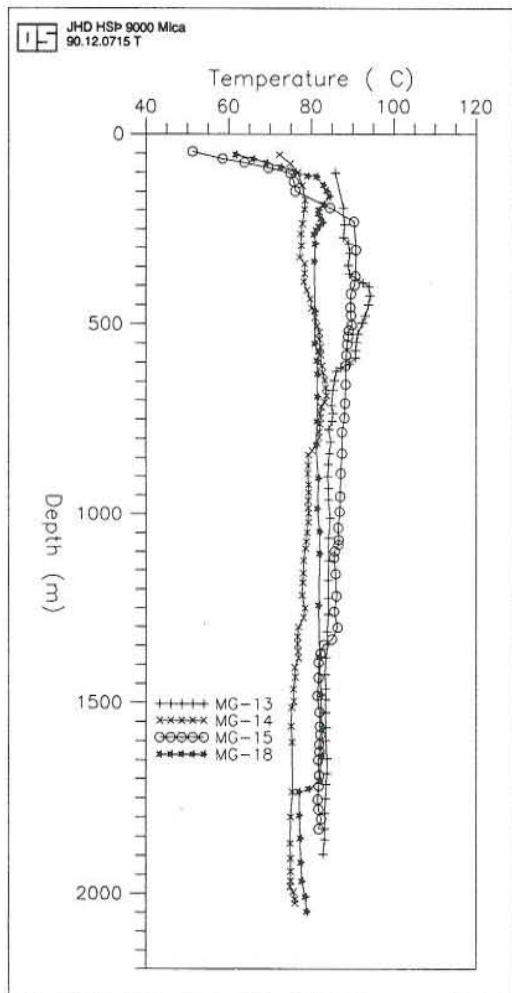


FIGURE 6: Temperature profiles of the wells in Reykir

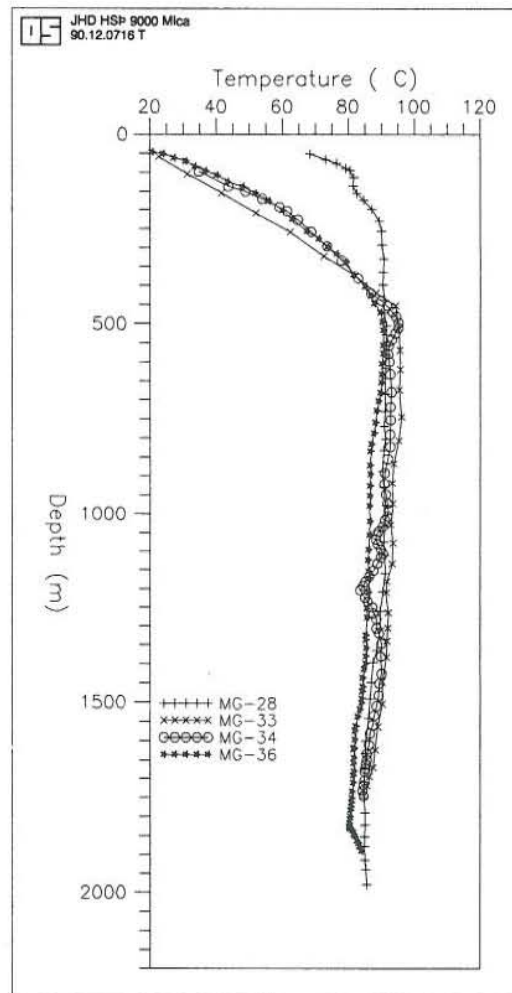


FIGURE 7: Temperature profiles of the wells in Reykjahlid

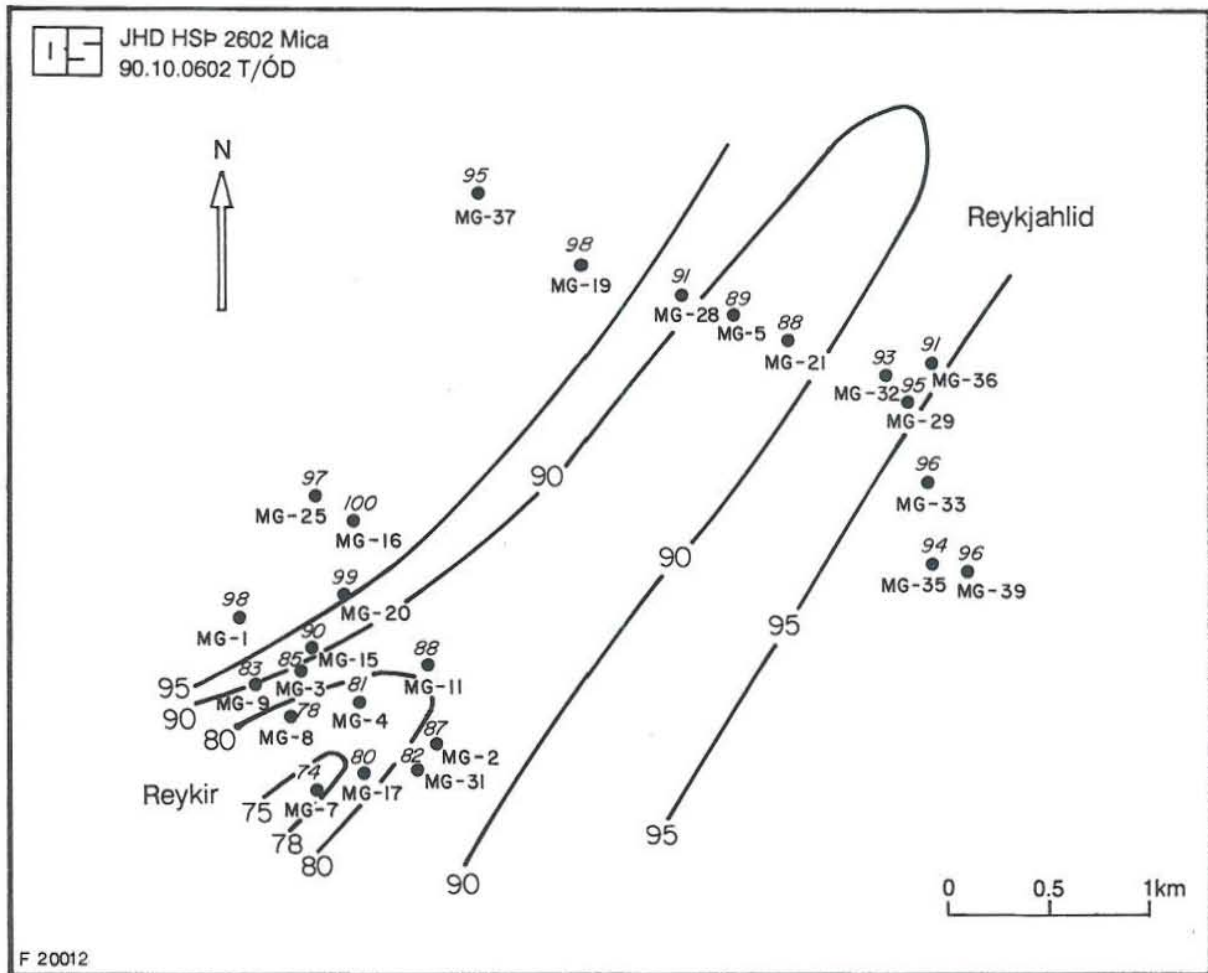


FIGURE 8: Map of maximum temperatures in Mosfellssveit geothermal field (Zhou Xi-Xiang, 1980)

2.4 Geophysics

The map with true resistivity at 900 m is shown in Figure 4 and the Bouguer anomalies gravity map in Figure 5. A general northeast-southwest structure can be seen in the low resistivity areas, which is in agreement with the trend of the hyaloclastite ridges. The old central volcanoes Kjalarnes and Stardalur are in the area of positive gravity anomalies which reflect the intensity of intrusions in the strata. The geological structure at the outskirts of the calderas makes it possible to have flow anisotropy direction along the boundaries. Geological mapping of the whole area reveals anisotropy in a north-northeasterly direction.

The results of the geophysical measurements indicate that the neo-volcanic zone could act as a constant head boundary condition for the geothermal fields, and no-flow boundary conditions are reached by approaching the tighter tertiary formations (Kjaran, 1986).

2.5 Temperature

The temperature measurements are taken from 39 wells in order to estimate the average temperature and the temperature distribution in the Reykir and Reykjahlid production fields (Zhou Xi-Xiang, 1980). The maximum temperature is usually between 200-1000 m depth. Deeper, the temperature decreases as depth increases. From the temperature curves which are shown in Figures 6 and 7, we can see a negative temperature gradient below 800-1000 m due to deep cold water recharge, mainly from the south-southwest. The horizontal flow of the thermal water appears to be at the depth interval of 200-1000 m, one part coming from the northwest, and the other from the southeast (Zhou Xi-Xiang, 1980).

The average estimated temperature is 83°C for Reykir and 91°C for Reykjahlid. The measurements for estimation of the average temperatures taken from the wellhead during production are taken as average temperatures for current wells for the last 15 years (Reykjavik Municipal Heating Service, 1985). Figure 8 shows the distribution of the maximum temperatures in the Mosfellssveit geothermal field.

2.6 Production history

Since 1944, the Mosfellssveit geothermal field has been the main source of thermal water supplying the Reykjavik heating service. Before 1933, the natural hot springs in the area discharged 120 l/s of thermal water by free flow. Until 1955, free flow was increased by 43 shallow wells at Reykir and 26 wells at Reykjahlid and reached a production of 360 l/s with a temperature of 86°C. Between 1970 and 1977, 37 wells, 800-2043 m deep, were drilled 22 and 34 cm in diameter. At the beginning of 1975, production from 20 pumped wells reached 851 l/s with an average temperature of 83.5°C. Due to greater production, the water level from relatively steady-state conditions with free flow declined by 20-35 m and eliminated free flow from the area. In 1989, the average production per year for the Mosfellssveit geothermal field was 1189 l/s, which gives 37.5 GJ. The production from Reykir field was 700 l/s, with an average temperature of 83°C. From the Reykjahlid geothermal field, the average production was 500 l/s with an average temperature of 91°C. If all the wells from both fields are in production, it is possible to yield 1799 l/s (data from Reykjavik District Heating Service). Figures 9, 10 and 11 show the production for each field, and the sum of the production for both fields from 1971 to 1989. Tables 2 - 4 show the same thing in numbers.

TABLE 2: Reykir, monthly production in m³, 1971-1989

year	JAN.	FEB.	MAR.	APR.	MAY	JUN.	JUL.	AUG.	SEP.	OCT.	NOV.	DEC.	sum
1971	0	0	0	292571	367174	261575	269234	129481	46254	228968	410117	392957	2398331
1972	538121	513834	549199	574743	418334	315755	406239	580498	658332	679098	720400	763750	6718303
1973	909235	859193	816751	796217	755256	816109	710529	797094	772050	947213	1155620	1387250	10722517
1974	1465638	1310720	1415640	1255700	1267750	1227750	1060140	814680	899761	1248850	1380540	1840590	15187759
1975	2034128	1857276	2015775	1921688	1611116	1209959	1037997	1189130	1254894	1520121	1815827	2389024	19856935
1976	2579380	2326899	2424470	2380319	2198191	1423827	1277950	1436369	1474174	1842696	2008009	2261082	23633366
1977	2036062	1741924	1917844	1509384	1287626	1186876	967523	1106512	1531398	1346897	1918063	1746959	18297068
1978	2118675	1772608	1589708	1393731	1713593	1711997	1437529	1492325	1820753	2059352	1764554	1738716	20613541
1979	1651083	1257555	1630968	1283292	1535690	1363502	1667830	1276049	1555118	1646512	1974875	2023381	18865855
1980	1988535	1769875	1760173	1581000	1251180	646620	1393111	1217600	1101433	1529477	1632347	1745484	17616835
1981	1929925	1683910	1590400	1178418	1364877	1540200	1504638	1623234	1329409	1570948	1724691	1831959	18872609
1982	1995055	1646530	1801470	1477236	1301185	1234502	1092837	1336213	1821061	1602837	1858592	1880867	19048385
1983	1978487	1320076	1518787	1335418	1239355	1808638	1641343	1842648	1708906	1702801	1478830	1755543	19330832
1984	2043703	1759400	1667552	1445984	1400575	1523231	1601014	1594207	1424852	1487220	1160339	1438206	18546283
1985	1680000	1410000	1640000	1540000	1510000	1650000	1600000	1130000	1080000	1210000	1660000	1910000	18020000
1986	1900000	1580000	1650000	1330000	1260000	990000	620000	1580000	1670000	1800000	1760000	1950000	18090000
1987	1720000	1550000	1820000	1400000	1640000	1520000	1640000	1580000	1150000	1370000	1470000	1420000	18280000
1988	2213248	2064065	1731657	1885614	1400165	1169421	681234	749896	960231	1296448	1408551	1736815	17297345
1989	1999866	1990559	2052832	1694457	1703382	1154607	1092933	914540	1617582	1493679	1874541	1916178	19505157

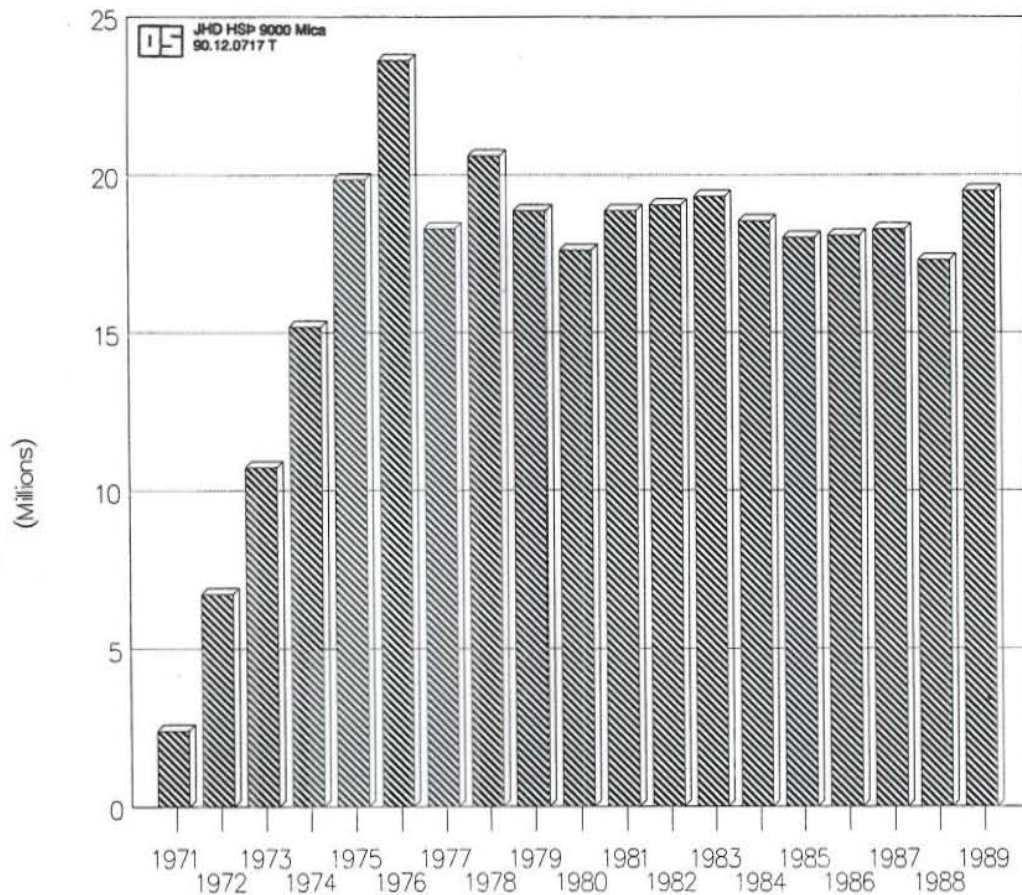
FIGURE 9: Reykir, annual production in m³, 1971-1989

TABLE 3: Reykjahlid, monthly production in m³, 1971-1989

year	JAN.	FEB.	MAR.	APR.	MAY	JUN.	JUL.	AUG.	SEP.	OCT.	NOV.	DEC.	sum
1974	0	0	0	9323	144520	139854	144482	144479	139800	144800	139800	144796	1151854
1975	144514	129435	136222	124400	139800	139800	144480	139979	137470	120539	132314	134854	1623807
1976	130282	105643	119982	116115	119982	116115	119982	119982	116185	88545	434871	513606	2101290
1977	758779	674477	746743	788990	752260	423470	301210	183163	360733	853250	814200	973147	7630422
1978	1177950	1135390	1167360	1229790	446628	0	31210	0	86643	505261	984473	1332570	8097275
1979	1929600	1665600	1716130	1377710	965278	528864	17162	260653	824836	1018180	937607	1079730	12321350
1980	1203140	1086410	1100050	980094	1035760	633272	41423	185430	555212	1196760	1292120	1653820	10963491
1981	1709440	1487050	1756210	1068940	664569	164791	171804	154477	175391	1164110	1636390	1923080	12076252
1982	1845550	1504680	1686030	844656	786560	538856	818744	1041000	1418060	1442210	1479190	1663840	15069376
1983	1643670	1698230	1719320	1706920	993187	31492	302	302	111425	956444	1522040	1568860	11952192
1984	1971460	1789740	1641290	1600900	1172690	397761	119834	140348	893044	1348910	1795730	1804220	14675927
1985	1770000	1740000	1800000	1230000	370000	0	0	770000	920000	1010000	1580000	1780000	12970000
1986	1870000	1420000	1760000	1460000	980000	920000	840000	180000	400000	1230000	1720000	1750000	14530000
1987	1610000	1500000	1750000	1580000	840000	0	0	0	950000	1680000	1550000	1450000	12910000
1988	2093480	1885400	1981951	1558191	1142539	858099	964410	1028481	1121412	1731136	1776360	1956937	18098396
1989	2025466	1912131	1897169	1595691	1640359	1027746	898244	1007760	996996	1461774	1591770	1858555	17913661

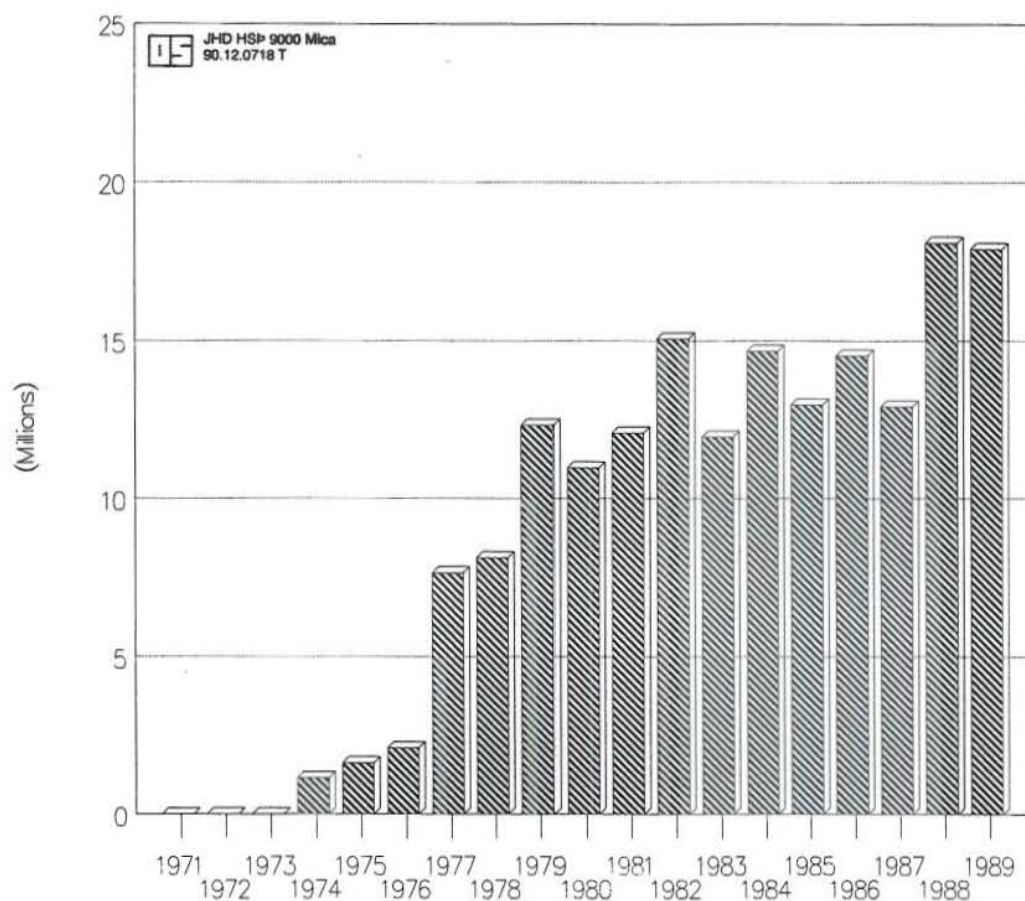
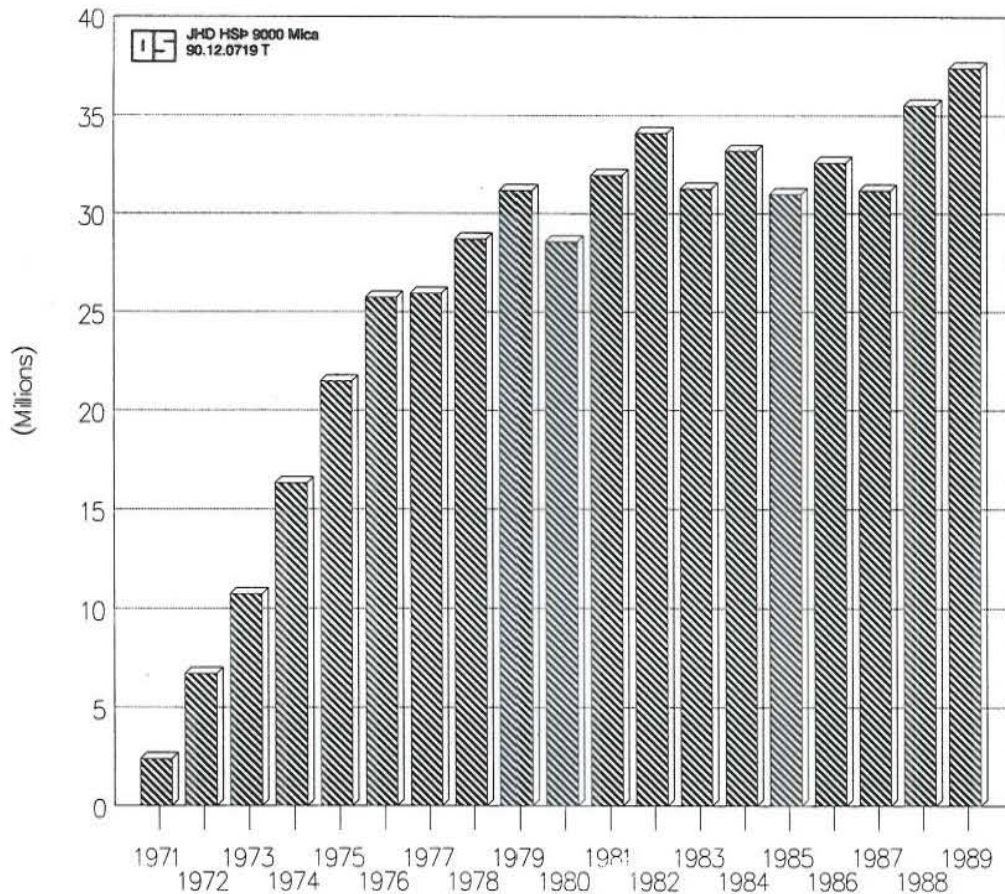
FIGURE 10: Reykjahlid, annual production in m³, 1971-1989

TABLE 4: Mosfellssveit, monthly production in m³, 1971-1989

year	JAN.	FEB.	MAR.	APR.	MAY	JUN.	JUL.	AUG.	SEP.	OCT.	NOV.	DEC.	sum
1971	0	0	0	292571	367174	261575	269234	129481	46254	228968	410117	392957	2398331
1972	538121	513834	549199	574743	418334	315755	406239	580498	658332	679098	720400	763750	6718303
1973	909235	859193	816751	796217	755256	816109	710529	797094	772050	947213	1155617	1387248	10722512
1974	1465638	1310720	1415644	1265020	1412274	1367603	1204625	959160	1039561	1393646	1520339	1985383	16339613
1975	2178643	1986711	2151998	2046088	1750916	1349759	1182477	1329109	1392365	1640660	1948142	2523878	21480746
1976	2709662	2432542	2544452	2496434	2318173	1539942	1397932	1556351	1590359	1931242	2442880	2774689	25734658
1977	2794842	2416401	2664588	2298374	2039886	1610346	1268733	1289675	1892131	2200147	2732263	2720107	25927493
1978	3296627	2907998	2757069	2623523	2160221	1711997	1468739	1492325	1907397	2564614	2749027	3071284	28710821
1979	3580679	2923151	3347094	2661006	2500968	1892366	1684993	1536702	2379955	2664689	2912482	3103115	31187200
1980	3191670	2856284	2860218	2561095	2286941	1279902	1434535	1403030	1656646	2726234	2924471	3399301	28580327
1981	3639363	3170962	3346610	2247361	2029446	1704991	1676443	1777711	1504801	2735055	3361084	3755039	30948866
1982	3840605	3151210	3487500	2321892	2087746	1773359	1911582	2377214	3239123	3045043	3337786	3544704	34117764
1983	3622152	3018309	3238110	3042334	2232543	1840130	1641645	1842951	1820332	2659245	3000873	3324405	31283029
1984	4015162	3549140	3308838	3046888	2573267	1920992	1720849	1734556	2317897	2836130	2956070	3242425	33222214
1985	3450000	3150000	3440000	2770000	1880000	1650000	1600000	1900000	2000000	2220000	3240000	3690000	30990000
1986	3770000	3000000	3410000	2790000	2240000	1910000	1460000	1760000	2070000	3030000	3480000	3700000	32620000
1987	3330000	3050000	3570000	2980000	2480000	1520000	1640000	1580000	2100000	3050000	3020000	2870000	31190000
1988	4306728	4023182	3771330	3443805	2542704	2027520	1645644	1778377	2081643	3027584	3184911	3693752	35527179
1989	4025331	3902690	3950001	3290148	3343741	2182353	1991177	1922301	2614578	2955453	3466311	3774734	37418818

FIGURE 11: Mosfellssveit, annual production in m³, 1971-1989

2.7 Utilization

The Reykjavik heating system serves a total population of about 120,000. The thermal water is taken from three geothermal fields: Laugarnes (330 l/s, 127°C) and Ellidaár (218 l/s, 93°C) which are in the city area, and Mosfellssveit (1200 l/s, 86°C) at 15-20 km distance. Due to the higher temperature of the water obtained in Reykjavik, its useful heat value is 47% that of the water from Mosfellssveit, although its volume is only 30% (Reykjavik District Heating Service, 1990) (Figure 12).

The thermal water from Reykir and Reykjahlid geothermal fields is pumped to the storage tanks in Reykjavik through two parallel 14" and 28" steel pipes, laid into a concrete conduit 17 km long. From the the storage tanks, water is pumped to the district pumping stations and then to consumers through either single or double pipe distribution systems. The water in the single pipeline is wasted after use, whereas the double pipeline returns the used fluid to the pumping stations where it is mixed with higher temperature water for reuse. The supply temperature provided to the consumer is about 80°C.

In order to calculate the thermal power of The Mosfellssveit geothermal field, it was assumed that the average inlet temperature of the water is 86°C and the outlet temperature is 35°C, which gives the following thermal power.

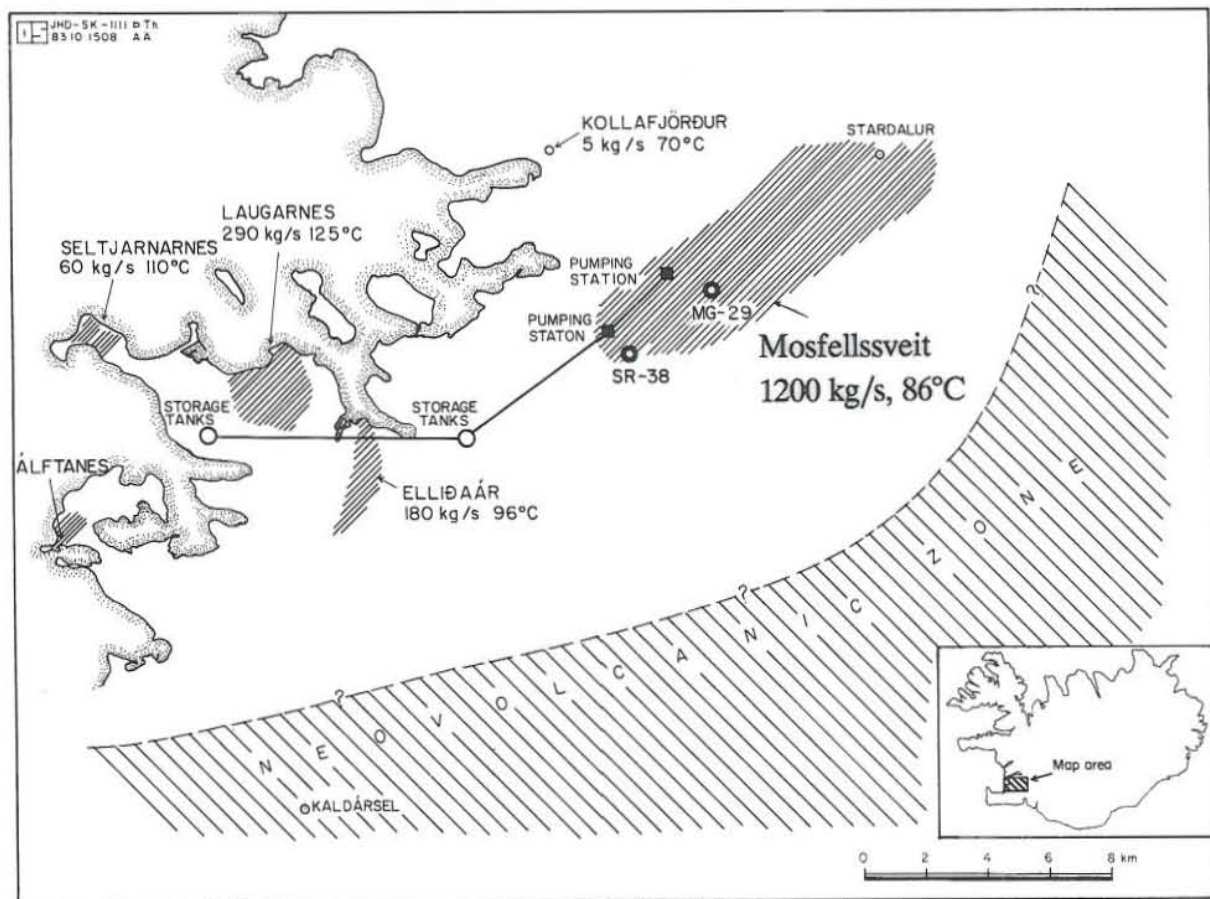


FIGURE 12: Location map of the Reykjavik low temperature fields

Total mass flow is given by:

$$T_m = m / v_f \quad (1)$$

T_m - total mass (kg/s)
 m - mass flow (l/s)
 v_f - specific volume (l/kg)

Total enthalpy for the inlet and outlet water is given by:

$$TE_i = T_m E_i \quad (2)$$

$$TE_o = T_m E_o \quad (3)$$

TE_i - total enthalpy of the inlet water

TE_o - total enthalpy of the outlet water

E_i - enthalpy of inlet water with temperature of 86 °C

E_o - enthalpy of outlet water with temperature of 35 °C

The thermal power for the field, taking into account only the temperature range which can be used, is given by:

$$P_t = TE_i - TE_o \quad (4)$$

P_t - Thermal power (MW)

The calculated used thermal power of The Mosfellssveit geothermal field is 372 MW.

3. LUMPED PARAMETER MODEL

3.1 General overview

Detailed numerical modelling of geothermal reservoirs is time consuming, costly, and requires large amounts of field data. Lumped parameter modelling is, in some cases, a cost effective alternative. A method has been developed that tackles simulation of pressure response data by lumped models as an inverse problem and, therefore, requires very little time. This lumped modelling method has been used successfully to simulate data from several low temperature geothermal reservoirs in Iceland. The lumped simulators provide information on the global hydrological characteristics of the geothermal reservoir and have been used to predict future pressure changes (Gudni Axelsson, 1989).

Lumped parameter models use two (or more) blocks to represent the entire system. One of the blocks represents the main reservoir or the productive area and the others act as recharge blocks. The governing equations for these models can often be reduced to ordinary differential equations that can be solved semi-analytically. Lumped parameter models are generally calibrated against the pressure history and average production from the field. After a historical match is obtained, the model is used to predict future water level with the present production rate.

The main advantages of the lumped parameter models are their simplicity and the fact that they do not require the use of large computers. The disadvantages of the lumped parameters are that they do not consider fluid flow within the reservoir and neglect spatial variations in thermodynamic conditions and reservoir properties. They cannot match the average enthalpy and noncondensable gas content of the produced fluids because of the large gridblock size. They cannot simulate fronts, such as phase or thermal fronts, because of the coarse space discretization. They cannot consider questions of well spacing or injection well locations (Bodvarsson, 1987).

3.2 Theoretical basis

In order to simulate a pressure response of the Mosfellssveit geothermal field, a simple lumped model with two reservoirs or two blocks is used. A simplified sketch of the lumped model is shown in Figure 13, mainly to give physical meaning to the applied approach and equations used.

The continuity of mass for two aquifers or two reservoirs could be expressed as follows:

$$Q_1 = \gamma_1(h_o - h_1) - A_1 S_1 \frac{dh_1}{dt} - \gamma_2(h_1 - h_2) \quad (5)$$

$$Q_2 = \gamma_2(h_1 - h_2) - A_2 S_2 \frac{dh_2}{dt} \quad (6)$$

The drawdowns for the aquifers are given by:

$$s_1 = h_o - h_1 \quad ; \quad s_2 = h_o - h_2$$

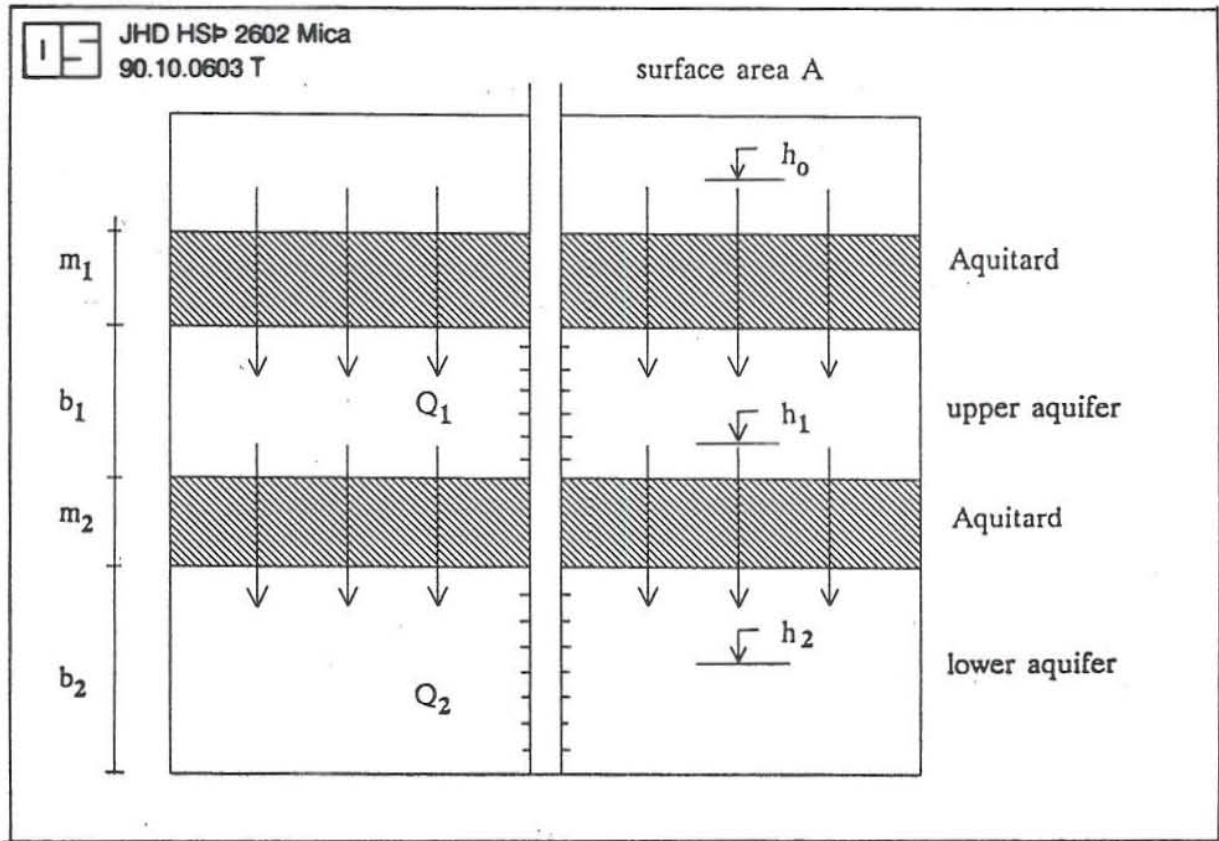


FIGURE 13: Simplified lumped two reservoir model

The parameters γ_1 and γ_2 are defined as:

$$\gamma_1 = \frac{K_1}{m_1} A_1 ; \gamma_2 = \frac{K_2}{m_2} A_2$$

This gives:

$$Q_1 - A_1 S_1 \frac{ds_1}{dt} + (\gamma_1 + \gamma_2) s_1 - \gamma_2 s_2 \quad (7)$$

$$Q_2 - A_2 S_2 \frac{ds_2}{dt} + \gamma_2 s_2 - \gamma_1 s_1 \quad (8)$$

where:

- $A_1 ; A_2$ - surface areas of the aquifers (m^2)
 b_1 - thickness, upper aquifer (m)
 b_2 - thickness, lower aquifer (m)
 h_0 - constant potential (m)
 h_1 - potential, upper aquifer (m)
 h_2 - potential, lower aquifer (m)
 m_1 - thickness, upper aquitard (m)
 m_2 - thickness, lower aquitard (m)
 K_1 - permeability, upper aquitard (m^2/s)
 K_2 - permeability, lower aquitard (m^2/s)
 s_1 - drawdown, upper aquifer (m)
 s_2 - drawdown, lower aquifer (m)
 S_1 - storage coefficient, upper aquifer
 S_2 - storage coefficient, lower aquifer
 Q_1 - pumping rate, upper aquifer (m^3/s)
 Q_2 - pumping rate, lower aquifer (m^3/s)

In order to solve Equations 7 and 8, the Laplace transform is used; then, equations for drawdowns in two reservoirs are obtained.

$$s_1 = \int_0^t Q_1(\tau) \left[\frac{1}{A_1 S_1} \frac{1}{(\lambda_2 - \lambda_1)} (\lambda_2 e^{-\lambda_2(t-\tau)} - \lambda_1 e^{-\lambda_1(t-\tau)}) + \frac{\gamma_2}{A_1 S_1 A_2 S_2} \frac{1}{\lambda_2 - \lambda_1} (e^{\lambda_1(t-\tau)} - e^{-\lambda_2(t-\tau)}) \right] d\tau + \frac{\gamma_2}{A_1 S_1 A_2 S_2} \int_0^t \frac{1}{\lambda_2 - \lambda_1} (e^{-\lambda_1(t-\tau)} - e^{\lambda_2(t-\tau)}) Q_2(\tau) d\tau \quad (9)$$

$$s_2 = \int_0^t Q_2(\tau) \left[\frac{1}{A_2 S_2} \frac{1}{(\lambda_2 - \lambda_1)} (\lambda_2 e^{-\lambda_2(t-\tau)} - \lambda_1 e^{-\lambda_1(t-\tau)}) + \frac{\gamma_1 + \gamma_2}{A_1 S_1 A_2 S_2} \frac{1}{\lambda_2 - \lambda_1} (e^{\lambda_1(t-\tau)} - e^{-\lambda_2(t-\tau)}) \right] d\tau + \frac{\gamma_2}{A_1 S_1 A_2 S_2} \int_0^t \frac{1}{\lambda_2 - \lambda_1} (e^{-\lambda_1(t-\tau)} - e^{\lambda_2(t-\tau)}) Q_1(\tau) d\tau \quad (10)$$

The parameters λ_1 and λ_2 are defined by the following equations:

$$\lambda_1 + \lambda_2 = \frac{\gamma_1 + \gamma_2}{A_1 S_1} + \frac{\gamma_2}{A_2 S_2} \quad (11)$$

$$\lambda_1 \lambda_2 = \frac{\gamma_1 + \gamma_2}{A_1 S_1 A_2 S_2} \quad (12)$$

If, for example only the lower aquaifer is producing, then:

$$Q_1 = 0 \quad ; \quad Q_2 = \text{constant} = Q$$

and the drawdown in the lower productive aquifer is given by:

$$s_2 = \frac{Q}{A_2 S_2} \frac{1}{\lambda_2 - \lambda_1} \left[e^{-\lambda_2(t-\tau)} - e^{-\lambda_1(t-\tau)} \right]_0^t + \frac{(\gamma_1 + \gamma_2) Q}{A_1 S_1 A_2 S_2} \frac{1}{\lambda_2 - \lambda_1} \left[\frac{1}{\lambda_1} e^{-\lambda_1(t-\tau)} - \frac{1}{\lambda_2} e^{-\lambda_2(t-\tau)} \right]_0^t \quad (13)$$

$$s_2 = \frac{Q}{A_2 S_2} \frac{1}{\lambda_2 - \lambda_1} + \left(\frac{\gamma_1 + \gamma_2}{A_1 S_1 \lambda_1} - 1 \right) (1 - e^{-\lambda_1 t}) + \frac{Q}{A_2 S_2} \frac{1}{\lambda_2 - \lambda_1} \left(1 - \frac{\gamma_1 + \gamma_2}{A_1 S_1 \lambda_2} \right) (1 - e^{-\lambda_2 t}) \quad (14)$$

$$s_2 = Q C_1 (1 - e^{-\lambda_1 t}) + Q C_2 (1 - e^{-\lambda_2 t}) \quad (15)$$

The coefficients C_1 and C_2 are given by:

$$C_1 = \frac{1}{A_2 S_2} \frac{1}{\lambda_2 - \lambda_1} \left(\frac{\gamma_1 + \gamma_2}{A_1 S_1 \lambda_1} - 1 \right) \quad (16)$$

$$C_2 = \frac{1}{A_2 S_2} \frac{1}{\lambda_2 - \lambda_1} \left(1 - \frac{\gamma_1 + \gamma_2}{A_1 S_1 \lambda_2} \right) \quad (17)$$

If we assume that $t \rightarrow \infty$ then, for steady-state conditions, the drawdown is given by:

$$s_2 = c_1 + c_2 = \frac{1}{A_1 S_1 A_2 S_2 \lambda_1 \lambda_2} \quad (18)$$

$$s_2 = \frac{1}{\gamma_1} + \frac{1}{\gamma_2}$$

The unit response function (URF) is given by:

$$F_2(t) = C_1 (1 - e^{-\lambda_1 t}) + C_2 (1 - e^{-\lambda_2 t}) \quad (19)$$

If the convolution approach with the superposition principle is used, then the drawdown in the lower aquifer is given by:

$$s_2(t) = \sum_{i=1}^n (Q_i - Q_{i-1}) F(t - t_{i-1}) \quad (20)$$

Based on Equation 20, the computer program UNITR4 was made in order to simulate the pressure response of the field with present production rates, and to calculate the parameters which represent the behaviour of the reservoir.

3.3 Results of the lumped parameter model

It was mentioned previously that a two reservoir model was used to simulate the pressure response data from the Mosfellssveit geothermal field. Water is produced from one of them and the other acts as a recharge reservoir.

This model is used mainly to simulate two different storage mechanisms. The storage coefficient, on one hand, might be controlled by liquid/formation compressibility, which is the case at the beginning of production; on the other hand, the storage coefficient might be controlled by the mobility of the free surface, which is the case in later production. At the same time the first reservoir could represent the vicinity of the well and short-term behaviour of the reservoir and the other could represent long-term behaviour and the recharge area.

A great amount of data is available from the fields, for example water level measurements, temperature measurements and measurements of the chemical content. For the lumped model, only the water level measurements are used for the calibration of the calculated and measured water levels.

Generally, if we take into account the whole reservoir, all measurements from the observation wells show approximately the same value, trend and fluctuations of the drawdown. The drawdown measurements for the fitting of the reservoir water level response are taken from the two observation wells, SR-15 and MG-28, mainly because of their continuity in observations for the last 20 years and the measured pressure response, which represents both fields if all measurements from observation wells are compared. The production rates are taken from 1971 to 1989 on a monthly basis in gigaliters (Gl) and recalculated in l/s.

After calibrating the model and fitting the calculated and measured water levels, the unit response function is calculated for a period of 30 years, from 1971 to 2000 (Figure 14).

The unit response function gives the value for the specific yield of the field as 12 l/s/m. But by comparing the seasonal fluctuation in the amplitude for the pumping rate to the water level, a yield of up to 25 l/s/m is obtained.

From the trend of the measured and calculated curve for the water level, it is quite obvious that with present production, no steady-state conditions can be reached until year 2000. So, the recharge in the system is much less than the production for the present drawdown. The measured and calculated water levels are shown in Figure 15. Calculated drawdown gives satisfactory fit with the measured drawdown.

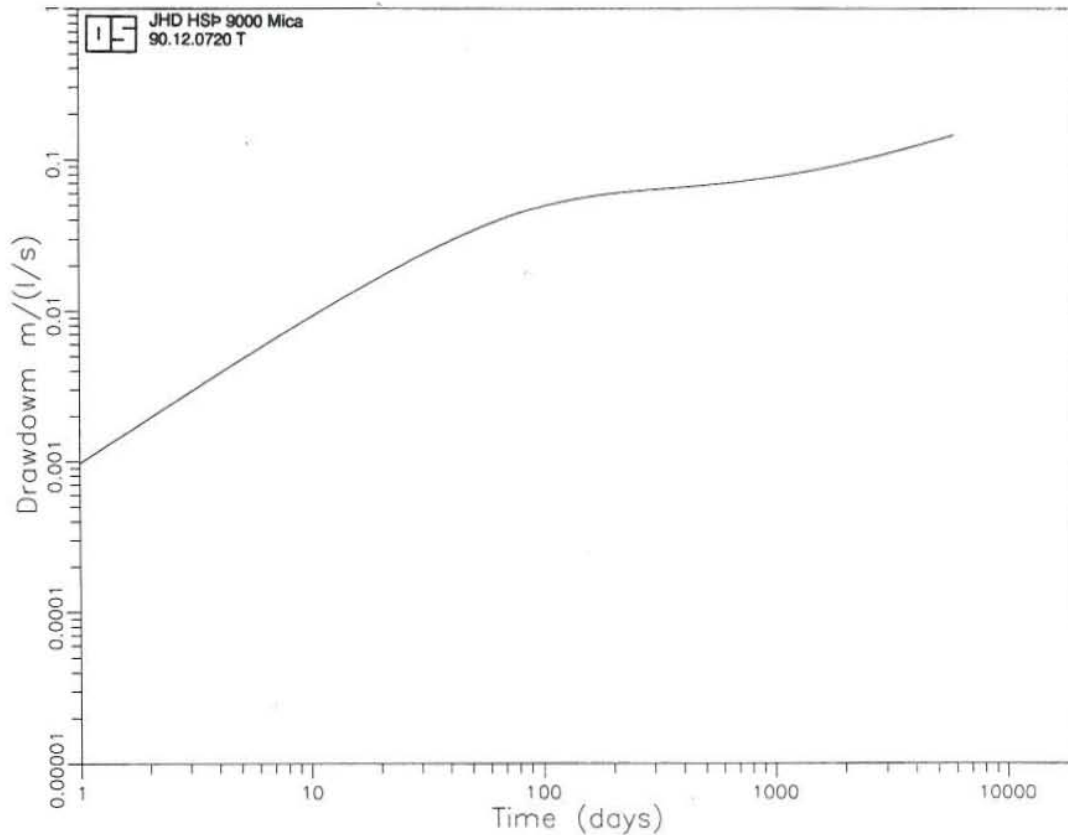


FIGURE 14: Unit response function

From the lumped model, the following parameters are obtained:

$$\lambda_1 = 1.9125 \text{ e}^{-7} \text{ s}^{-1}$$

$$\lambda_2 = 7.043 \text{ e}^{-10} \text{ s}^{-1}$$

$$C_1 = 58.25 \text{ m}$$

$$C_2 = 185.66 \text{ m}$$

3.4 Future prediction of the water level

A calibrated lumped model is used to predict future pressure response of the reservoir with different production rates. Prediction of the reservoir future behavior was based on the 1989 production year. The average production for the whole year was 1189 l/s. During the winter months the production reached 1613 l/s in February, near to the maximum (1799 l/s) possible to produce from the wells. During the summer months production was between 700 and 800 l/s. Due to differences in the amount of pumped water during winter and summer, changes in the water level were between 25-30 m.

In order to predict future pressure response of the reservoir, three different assumptions or future prediction cases are established.

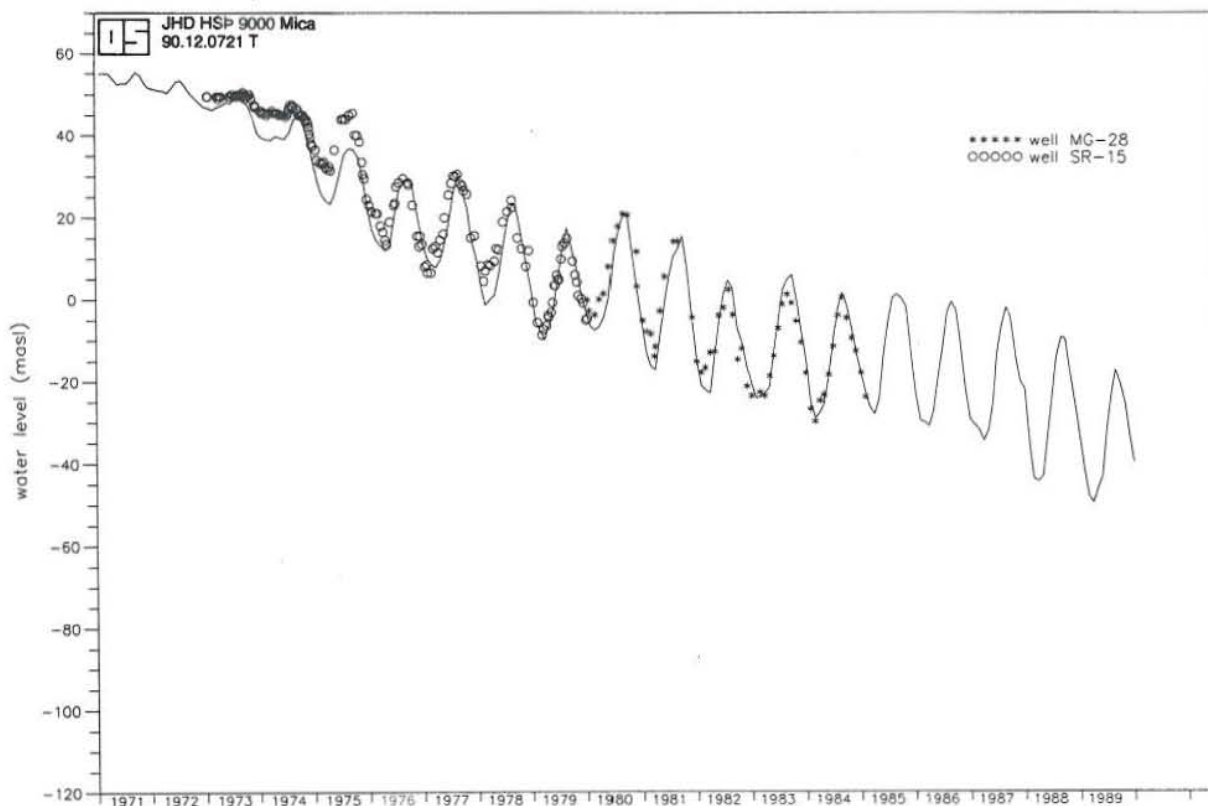


FIGURE 15: Measured and calculated drawdown for the Mosfellssveit geothermal field

3.4.1 Future prediction, case 1

Future prediction for the next 10 years (until year 2000) for case 1 is based on the same monthly production rates as for year 1989 (Figure 16). The results of the model are shown in Figure 17. The drawdown after a period of 10 years, will reach 135 m or -80 m (amsl), with no steady-state conditions. The lowering of the water level is approximately 3 m per year, with the same trend for the future. The difference between maximum and minimum water levels during the winter and summer months is 25-30 m, due to different production rates.

3.4.2 Future prediction, case 2

The monthly production rates for future prediction case 2 are shown in Figure 18. The same production rates are used as in the previous model for the winter months but only half of the production rates for the summer months. The drawdown after 10 years will reach 125 m, with a lowering rate of approximately 2.5 m per year (Figure 19). The difference between the maximum and minimum water level is 40 m. The greater difference between the maximum and minimum water level, compared to the previous model, is due to lower production during the summer months.

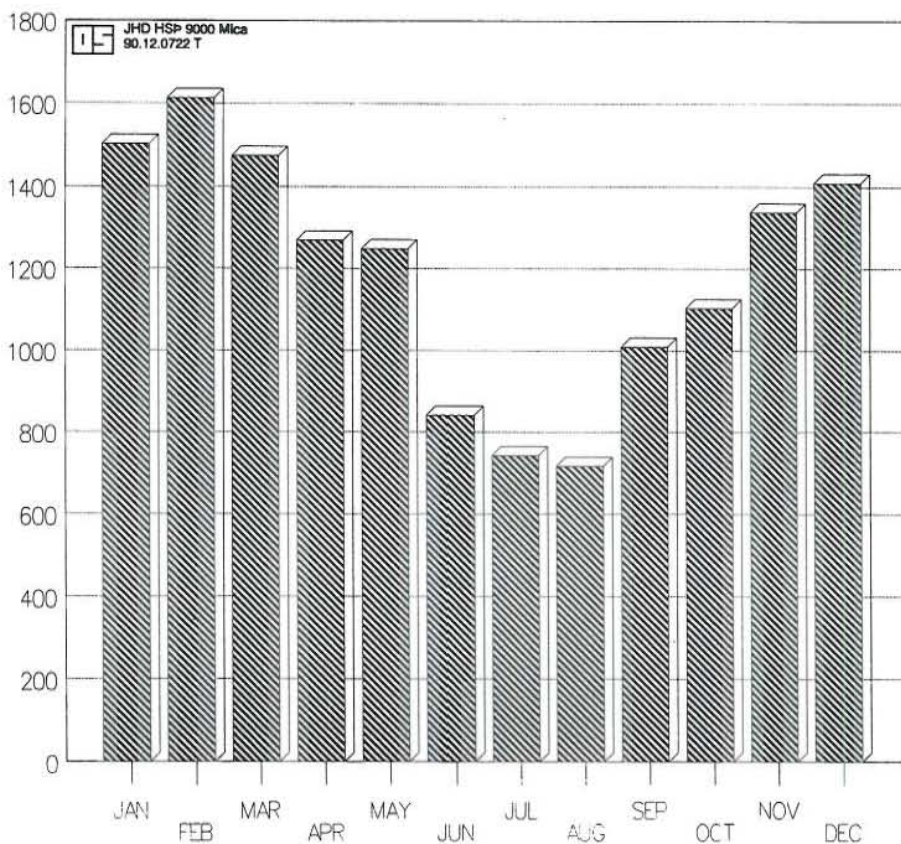


FIGURE 16: Mosfellssveit - monthly production 1989 in $10^3 \times m^3$

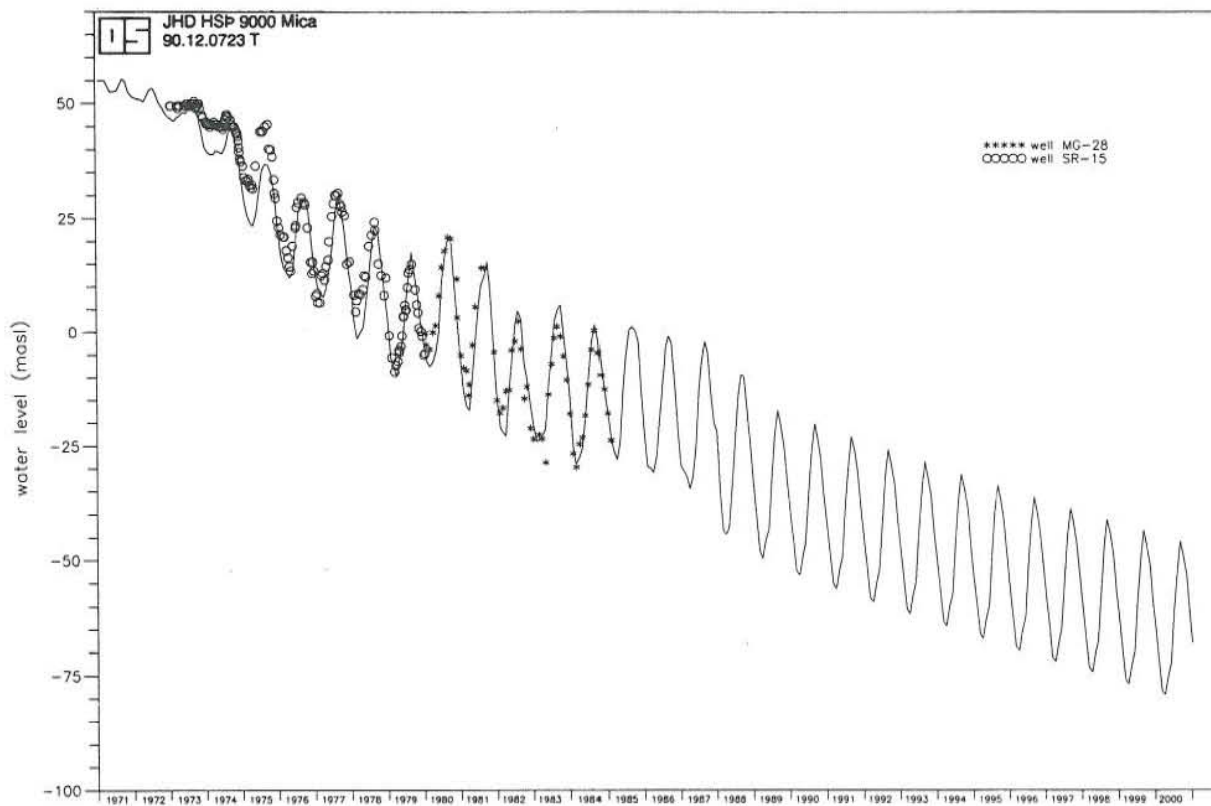


FIGURE 17: Future prediction, case 1

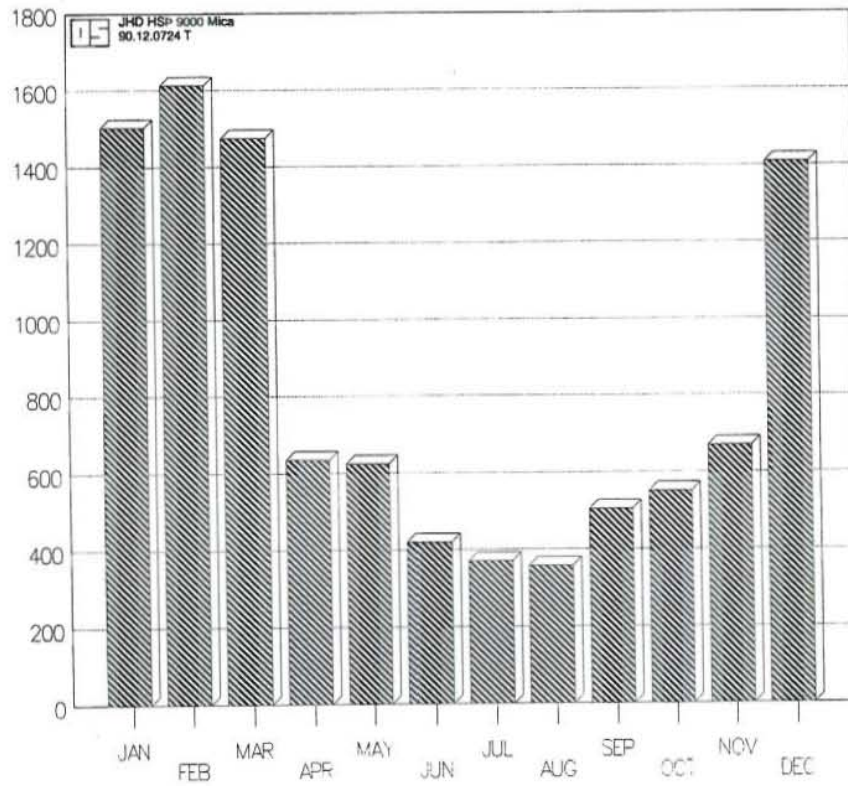


FIGURE 18: Mosfellssveit - monthly production in $10^3 \times m^3$, used for case 2

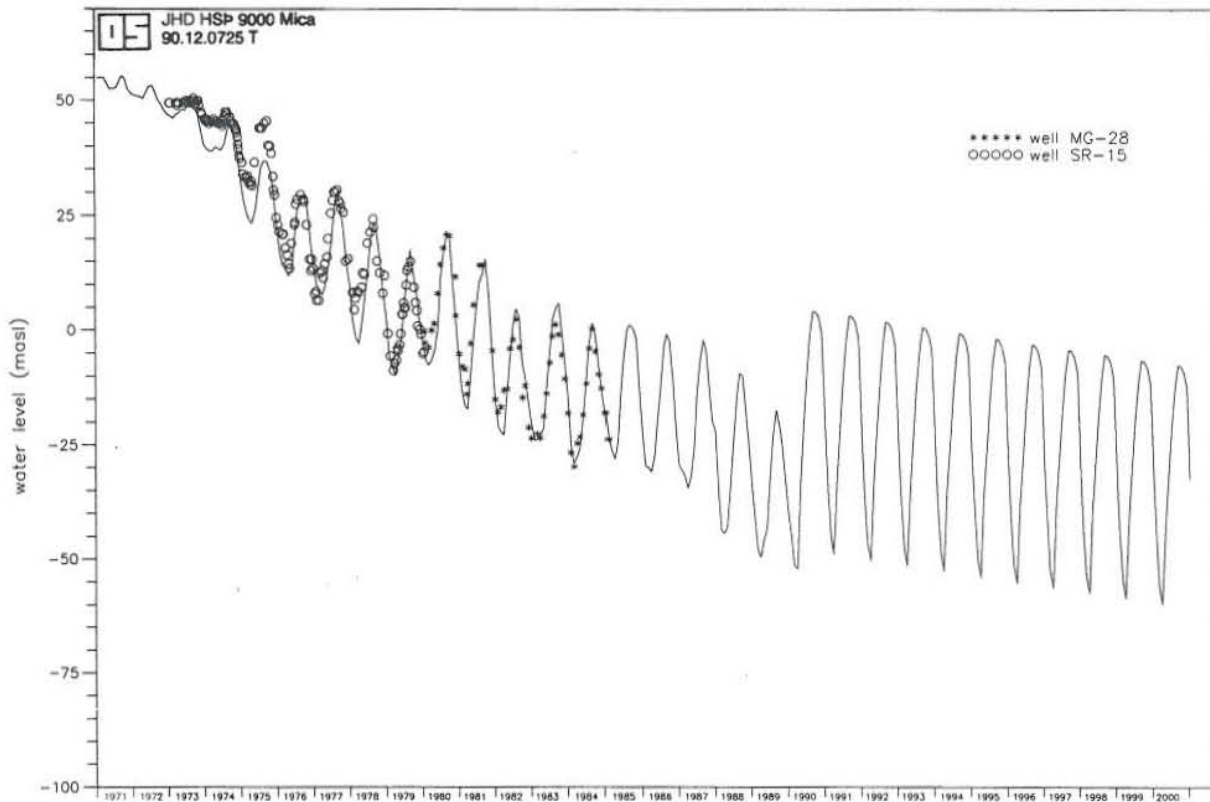


FIGURE 19: Future prediction, case 2

3.4.3 Future prediction, case 3

Future prediction for case 3 is made in order to estimate the future pressure response of the reservoir with different production rates for the next 10 years. The calculations are made with nine different production rates in the range between 400 and 1300 l/s. For the previous assumption, calculated water level has an average value and fluctuations are neglected. Table 5 shows the results of the calculations. The drawdown of 94.72 m in year 1989 was a beginning value for the calculations of the future water levels for the next 10 years.

All calculated curves with greater production than 500 l/s, show a lowering of the water level. The calculated drawdown in the reservoir after 10 years will be between 42.34 m for the production of 400 l/s, and 131.01 m for the production of 1300 l/s (Figure 20). The obtained drawdowns have average values, and greater drawdowns could be expected during peaks in production. Relatively pseudo steady-state conditions or equilibrium between production and induced recharge with present drawdown could be reached with a production rate of 500 l/s and drawdown of 52 m.

TABLE 5: Calculated drawdowns with different annual production rates for next 10 years

year	1989	1990	1991	1992	1993	1994	1995	1996	1997	1998	1999	2000
PROD. (l/s)	D R A W D O W N (m)											
400	94.72	45.46	45.01	44.69	44.37	44.06	43.76	43.46	43.17	42.89	42.61	42.34
500	94.72	51.68	51.64	51.71	51.77	51.84	51.90	51.96	52.02	52.08	52.14	52.19
600	94.72	57.90	58.27	58.73	59.18	59.62	60.04	60.46	60.87	61.27	61.66	62.05
700	94.72	64.11	64.90	65.75	66.58	67.39	68.19	68.96	69.72	70.46	71.19	71.90
800	94.72	70.33	71.54	72.78	73.99	75.17	76.33	77.46	78.57	79.65	80.71	81.75
900	94.72	76.55	78.17	79.80	81.39	82.95	84.47	85.96	87.42	88.84	90.24	91.60
1000	94.72	82.77	84.80	86.82	88.80	90.73	92.61	94.46	96.27	98.03	99.76	101.45
1100	94.72	88.99	91.43	93.85	96.20	98.50	100.75	102.96	105.12	107.22	109.29	111.31
1189	94.72	94.52	97.33	100.10	102.79	105.42	108.00	110.53	112.99	115.40	117.76	120.07
1300	94.72	101.43	104.69	107.89	111.01	114.06	117.04	119.96	122.82	125.61	128.33	131.01

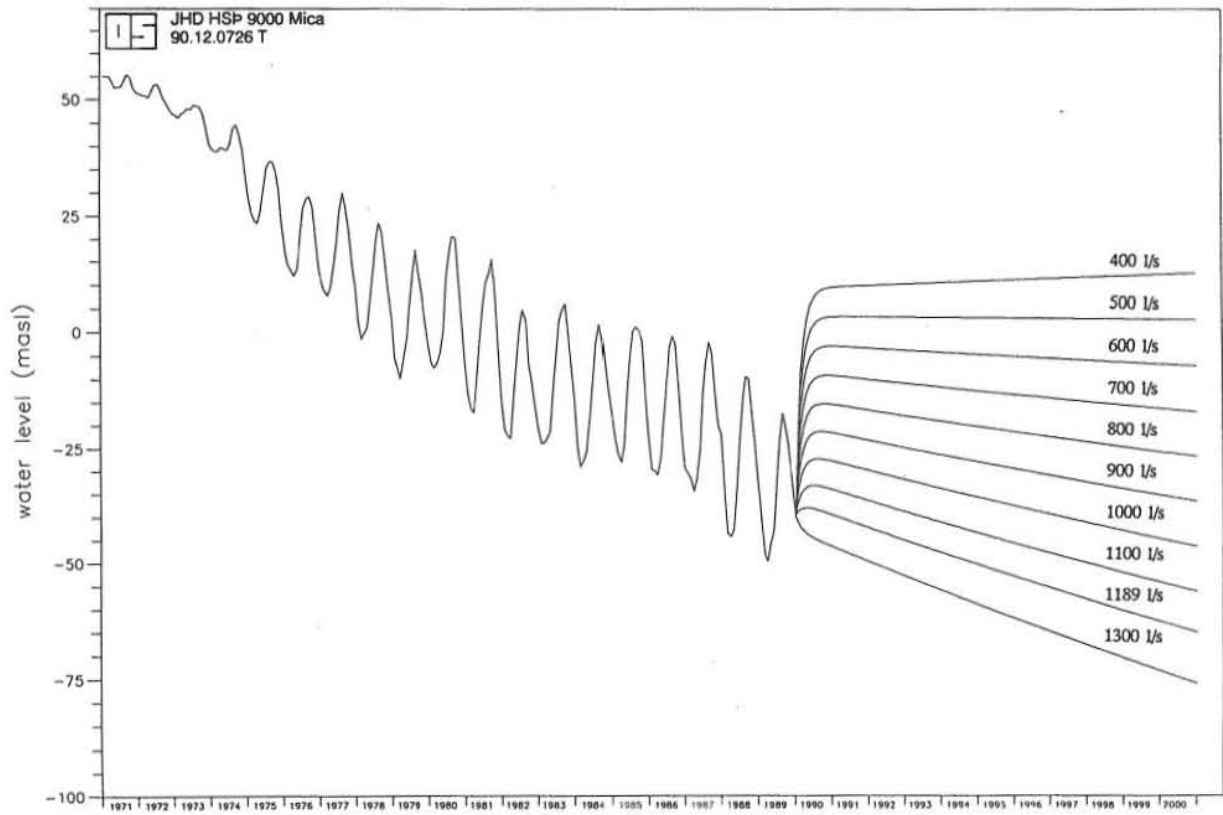


FIGURE 20: Future prediction, case 3

4. DISTRIBUTED PARAMETER MODEL

4.1 General overview

Distributed parameter models are very general models that can be used to simulate reservoirs with few (equivalent to lumped parameter models) or many (> 100 to 1000) gridblocks. They can be used to simulate the entire geothermal system including reservoir, caprock, bedrock, shallow cold aquifers, recharge zones, etc. They allow for spatial variations in rock properties and thermodynamic conditions.

The principal advantage of the distributed parameter models is that they have all the mathematics built into a computer code and allow the user to decide how detailed (number of grid blocks) the simulation should be and what physical processes should be considered. Disadvantages of the distributed parameter models are the need for a large computer and an experienced modeller (Bodvarsson, 1987).

4.2 Theoretical basis with emphasis on the AQUA programme

The AQUA programme was used in order to make a distributed parameter model of the Mosfellssveit geothermal field. AQUA is a computer programme developed by Vatnaskil Consulting Engineers (1989) to solve groundwater flow, mass and heat transport equations using the Galerkin finite element method.

AQUA can be used on a IBM PC or compatible computers and requires the following hardware:

IBM PC/XT/AT or compatible
640K memory
EGA graphics card and display
Hard disk

The following differential equation forms the basis for establishing the mathematical model which can be then solved by AQUA:

$$a \frac{\sigma u}{\sigma t} + b_i \frac{\sigma u}{\sigma x_i} + \frac{\sigma}{\sigma x_i} (e_{ij} \frac{\sigma u}{\sigma x_j}) + fu + g = 0 \quad (21)$$

The model is two dimensional, and indices i and j indicate the x and y coordinate axes.

4.2.1 Flow model

For the transient groundwater flow, Equation 21 is reduced to:

$$a \frac{\sigma u}{\sigma t} + \frac{\sigma}{\sigma x_i} (e_{ij} \frac{\sigma u}{\sigma x_j}) + fu + g = 0 \quad (22)$$

For unconfined groundwater flow, Dupuit approximation and fully penetrating wells are assumed. The parameters in Equation 22 are defined as:

$$\begin{aligned} e_{ij} &= I_{ij} \\ f &= 0 \\ g &= Q + R \\ a &= -S \end{aligned}$$

Using x and y instead of the indices in Equation 22, the unconfined groundwater transient flow is defined as:

$$\frac{\sigma}{\sigma x} \left(T_{xx} \frac{\sigma h}{\sigma x} \right) + \frac{\sigma}{\sigma y} \left(T_{yy} \frac{\sigma h}{\sigma y} \right) + R + Q - S \frac{\sigma h}{\sigma t} \quad (23)$$

where:

$$\begin{aligned} h &- \text{groundwater head (m)} \\ T_{xx} &- \text{transmissivity along x-axis (m}^2\text{/s)} \\ T_{yy} &- \text{transmissivity along y-axis (m}^2\text{/s)} \\ R &- \text{infiltration (m/year)} \\ Q &- \text{pumping/injection rate (m}^3\text{/s)} \\ S &- \text{storage coefficient} \end{aligned}$$

For confined groundwater flow, the parameters in the Equation 22 are defined as:

$$\begin{aligned} u &= h \\ e_{ij} &= T_{ij} \\ f &= 0 \\ g &= Q + \left(\frac{k}{m} \right) h_0 \\ a &= -S \end{aligned}$$

which gives the following equation for confined groundwater flow:

$$\frac{\sigma}{\sigma x} \left(T_{xx} \frac{\sigma}{\sigma x} \right) + \frac{\sigma}{\sigma y} \left(T_{yy} \frac{\sigma x}{\sigma y} \right) + \frac{k}{m} (h_0 - h) + Q - S \frac{\sigma h}{\sigma t} \quad (24)$$

The ratio k/m defines the leakage coefficient where k is the permeability of the semi-permeable layer and m its thickness.

Two boundary conditions are used:

1. Dirichlet boundary conditions
2. Von Neumann boundary conditions

In the Dirichlet boundary conditions the groundwater level, the piezometric head or the potential function is prescribed at the boundary. In the von Neumann boundary condition the flow at the

boundary is prescribed. Given flow at the boundary can be modelled by putting sources (pumping) at the no-flow boundary nodes.

4.2.2 Mass transport model

The AQUA programme is able to solve transient transport of mass by using the properly defined parameters in Equation 21. Parameters are defined as follows:

$$\begin{aligned} u &= c \\ a &= \phi b R_d \\ b_i &= V_i b \\ e_{ij} &= \phi b D_{ij} \\ f &= \phi b R_d \lambda + Y + Q \\ g &= -Y c_0 - Q c_w \end{aligned}$$

By using x and y instead of the indices in Equation 21, the equation for transient transport of mass is given by:

$$\begin{aligned} \frac{\sigma}{\sigma x} \left(\phi b D_{xx} \frac{\sigma c}{\sigma x} \right) + \frac{\sigma}{\sigma y} \left(\phi b D_{yy} \frac{\sigma c}{\sigma y} \right) - u b \frac{\sigma c}{\sigma x} - v b \frac{\sigma c}{\sigma y} \\ - \phi b R_d \frac{\sigma c}{\sigma} t + \phi b R_d \lambda c - (c_0 - c) Y - Q (c_w - c) \end{aligned} \quad (25)$$

The above equation applies to a local coordinate system within each element having the main axis along the flow direction. The dispersion coefficients D_{xx} , D_{yy} are defined by:

$$\phi D_{xx} = a_L V^n + D_m \phi \quad (26)$$

$$\phi D_{yy} = a_T V^n + D_n \phi \quad (27)$$

The retardation coefficient R_d is given by:

$$R_d = 1 + \beta_1 (1 - \phi) \rho_s / (\phi \rho_l) \quad (28)$$

$$\beta_1 = K_d \rho_l \quad (29)$$

where:

- a_L - longitudinal dispersivity (m)
- a_T - transversal dispersivity (m)
- c - solute concentration (kg/m^3)
- c_0 - concentration of vertical inflow (kg/m^3)
- c_w - concentration of injected water (kg/m^3)
- h_0 - potential, upper aquifer (m)

- K_d - distribution coefficient
 D_m - molecular diffusivity (m^2/s)
 V - velocity (m/s)
 λ - exponential decay constant (s^{-1})
 ρ_l - density of the liquid (kg/m^3)
 ρ_s - density of the porous media (kg/m^3)
 β_1 - retardation coefficient
 Y - R (infiltration rate): unconfined horizontal aquifer
 $Y = \left(\frac{k}{m}\right)\left(\frac{h_0}{h}\right)$: confined horizontal aquifer

4.2.3 Heat transport model

Using the same base Equation 21, AQUA can solve single phase heat transport problems by proper selection of the parameters. They are defined as follows:

$$\begin{aligned}
 u &= T \\
 a &= \phi b R_h \\
 B_i &= V_i b \\
 e_{ij} &= -b K_{ij} \\
 f &= Y + Q \\
 g &= -Y T_0 - Q T_w
 \end{aligned}$$

By using x and y instead of the indices in Equations 21, the equation for single phase heat transport is given by:

$$\begin{aligned}
 &\frac{\sigma}{\sigma x} \left(b K_{xx} \frac{\sigma T}{\sigma x} \right) + \frac{\sigma}{\sigma y} \left(b K_{yy} \frac{\sigma T}{\sigma y} \right) - u b \frac{\sigma T}{\sigma x} - v b \frac{\sigma T}{\sigma y} - \\
 &\phi b R_h \frac{\sigma T}{\sigma t} - (T_0 - T) Y - (T_w - T) Q
 \end{aligned} \tag{30}$$

The above equation applies to a local coordinate system within each element having the main axis along the flow direction. The heat dispersion coefficients are given by:

$$K_{xx} = a_L V^n + D_h \phi \tag{31}$$

$$K_{yy} = a_T V^n + D_h \phi \tag{32}$$

The heat retardation coefficient R_h is given by:

$$R_h = 1 + \beta_2 (1 - \phi) \rho_s / (\phi \rho_l) \tag{33}$$

$$\beta_2 = \frac{C_s}{C_l} \quad (34)$$

where:

T - temperature ($^{\circ}\text{C}$)

ϕ - porosity

T_0 - temperature : vertical inflow ($^{\circ}\text{C}$)

C_l - specific heat capacity of the liquid (kJ/kg)

C_s - specific heat capacity of the porous media (kJ/kg)

β_2 - specific heat capacity coefficient

4.3 Basis of the model

4.3.1 Basic assumptions

The total surface area covered by the model is 162 km². Production from Reykir and Reykjahlid was simulated by two wells, each with a flow rate representing the total production from the respective fields. The production rates are taken on a monthly basis in l/s from 1971 to 1989. For matching the calculated and measured water levels, observations from well MG-1 (Reykir), SR-15, MG-28 (Reykjahlid) and S-1 (Stardalur) are taken into account.

4.3.2 Establishing the boundary conditions

Boundary conditions for the distributed groundwater flow model are established, based on resistivity, temperature and water level measurements. The main cold water recharge in the area comes from the south-southwest. According to the previous assumption, the southern boundary is established as a boundary with constant head conditions. The no-flow boundary is established in the west according to the water level measurements with no significant influence on the production in the Ellidaár geothermal field and the Mosfellssveit geothermal field. To the north of the area covered by the model, tighter formations (according to resistivity and gravity measurements) act as a no-flow boundary. To the east, a no-flow boundary is established at a distance of 10 km from the field (Figure 21).

4.3.3 Initial parameter values

The initial values for transmissivity and storage coefficient are taken from the results of well tests (Thorsteinsson, 1975). The range for transmissivity varies between 0.48 and 2.6 10⁻² m²/s, and for storage coefficient between 1.2 to 3.9 10⁻⁴.

Anisotropy is determined by anisotropy angle and by the ratio between transmissivity in x (T_{xx}) and y (T_{yy}) directions. Anisotropy angles are determined from geological mapping and gravity surveys. The initial ratio T_{xx}/T_{yy} is 10.

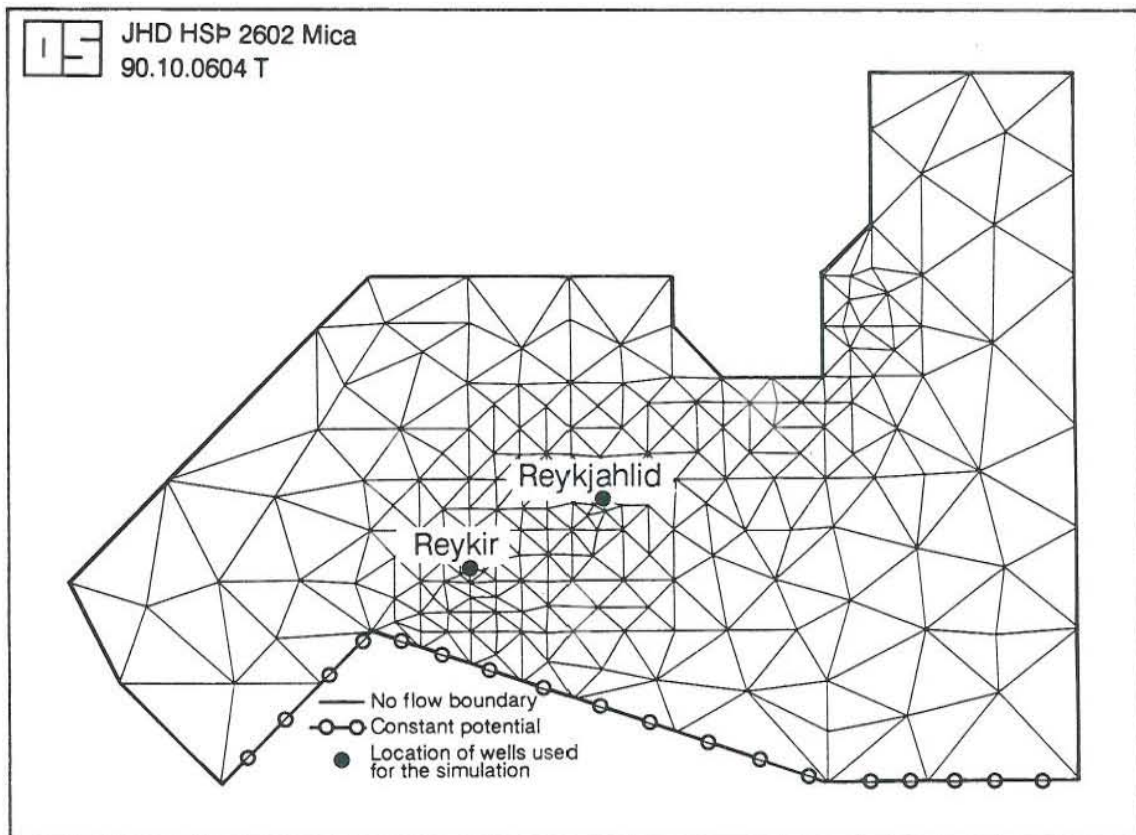


FIGURE 21: Boundary conditions of the model

According to the small influences on temperature and chemical content from cold water recharge from above, the initial value for the leakage coefficient around the productive area is established as $1 \cdot 10^{-12} \text{ s}^{-1}$.

4.4 Results of the distributed groundwater flow model

The transmissivity, storage coefficient and anisotropy are determined by matching observed and calculated reservoir responses.

4.4.1 Transmissivity

The transmissivity in the area covered by the model varies from $6 \cdot 10^{-5}$ to $2.4 \cdot 10^{-2} \text{ m}^2/\text{s}$ (Figure 22). The low value for transmissivity is obtained along the southern flow boundary of the model which indicates continuous small cold water recharge from the south. This cold water recharge can be seen on the temperature curves and it appears below 1000 m. The transmissivity in productive areas is $2.5 \cdot 10^{-2}$ (Reykjavik) and $2.1 \cdot 10^{-2} \text{ m}^2/\text{s}$ (Reykjahlid) which is near to the values obtained by Thorsteinsson (1975).

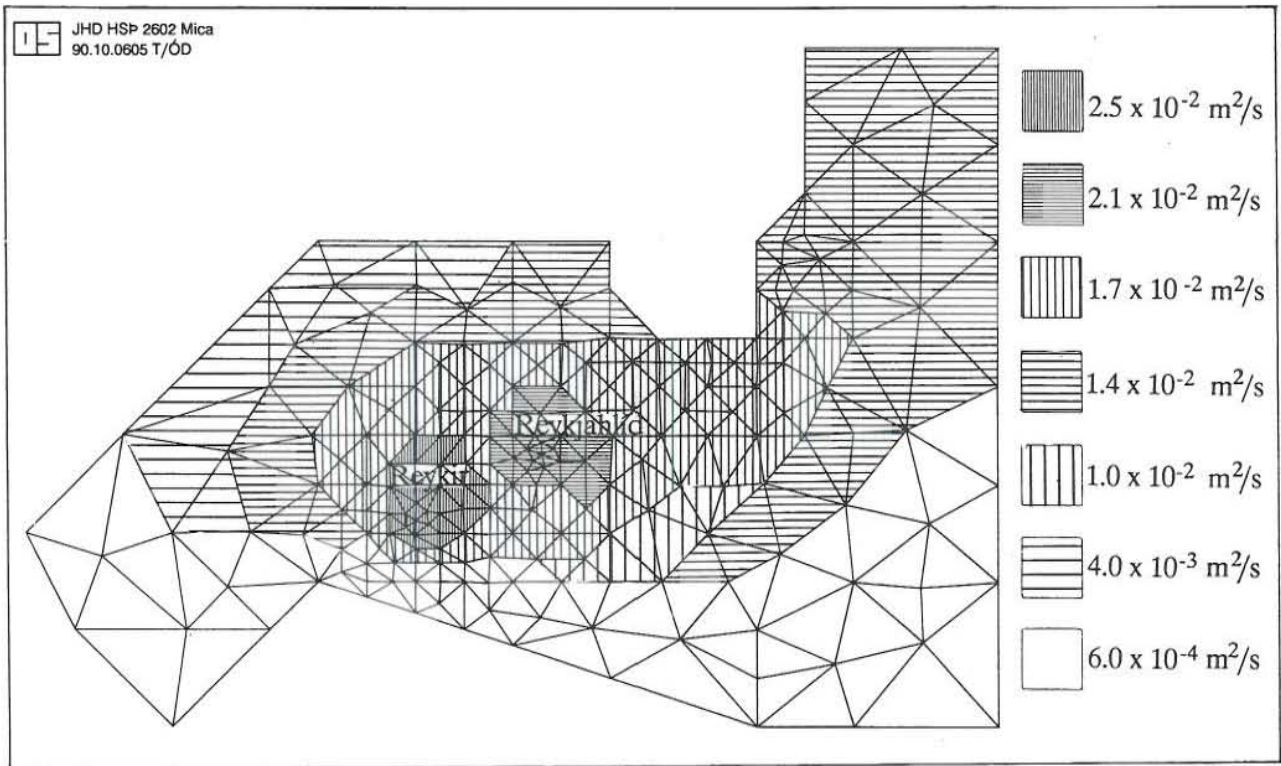


FIGURE 22: Map of transmissivities

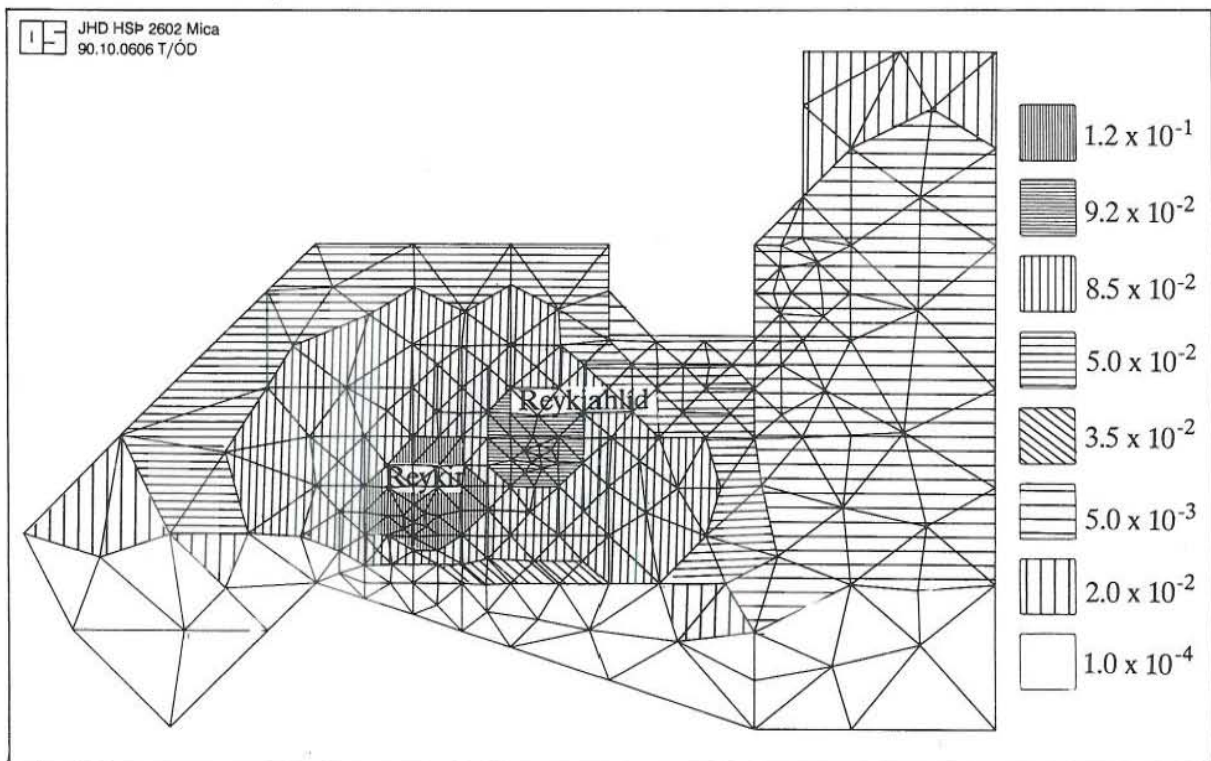


FIGURE 23: Map of storage coefficients

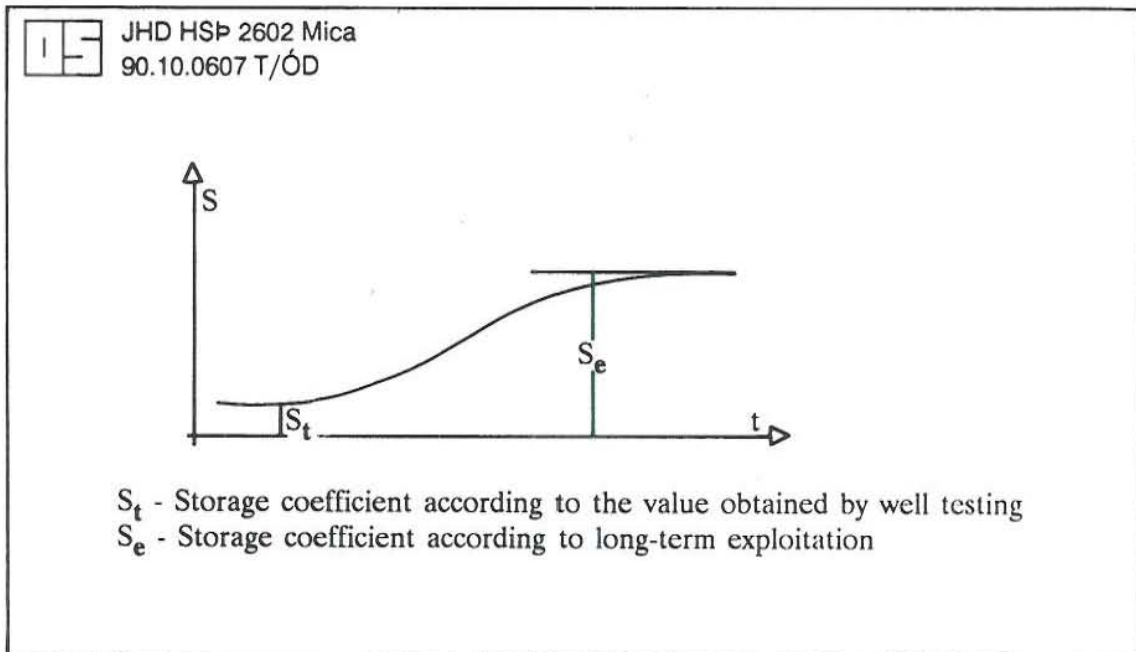


FIGURE 24: Changes in storage coefficient during exploitation

4.4.2 Storage coefficient

The obtained value for storage coefficient is very high if it is compared with the values calculated by well testing. In the productive areas, storage coefficient reaches a value of 0.12 in the Reykir geothermal field and 0.092 in the Reykjahlid geothermal field (Figure 23).

A great difference between storage coefficient obtained by the distributed model and storage coefficient obtained through well testing (Thorsteinsson, 1975) is possible to explain with two different storage mechanisms which appear during the exploitation of the field. At the start of production, storage coefficient is controlled by compressibility of the water and deformability of the rocks with the characteristic value for the confined aquifers. Later production and spreading of the drawdown cone induces bigger recharge into the system and an increase of storage coefficient, now controlled by effective porosity. The storage coefficient obtained by Thorsteinsson could characterize short-term behaviour of the reservoir and it represents the area in the vicinity of tested wells. The storage coefficient obtained by the distributed model characterized the whole productive area with a value which reflects long-term behaviour of the reservoir. During utilization of the reservoir, the increase of the storage coefficient is present, mainly due to delayed yield and double porosity effects. The ratio between the storage coefficient obtained at the start and in later utilization of the field could be from 1 up to 50. Figure 24 shows possible changes in storage coefficient through time during exploitation of the field.

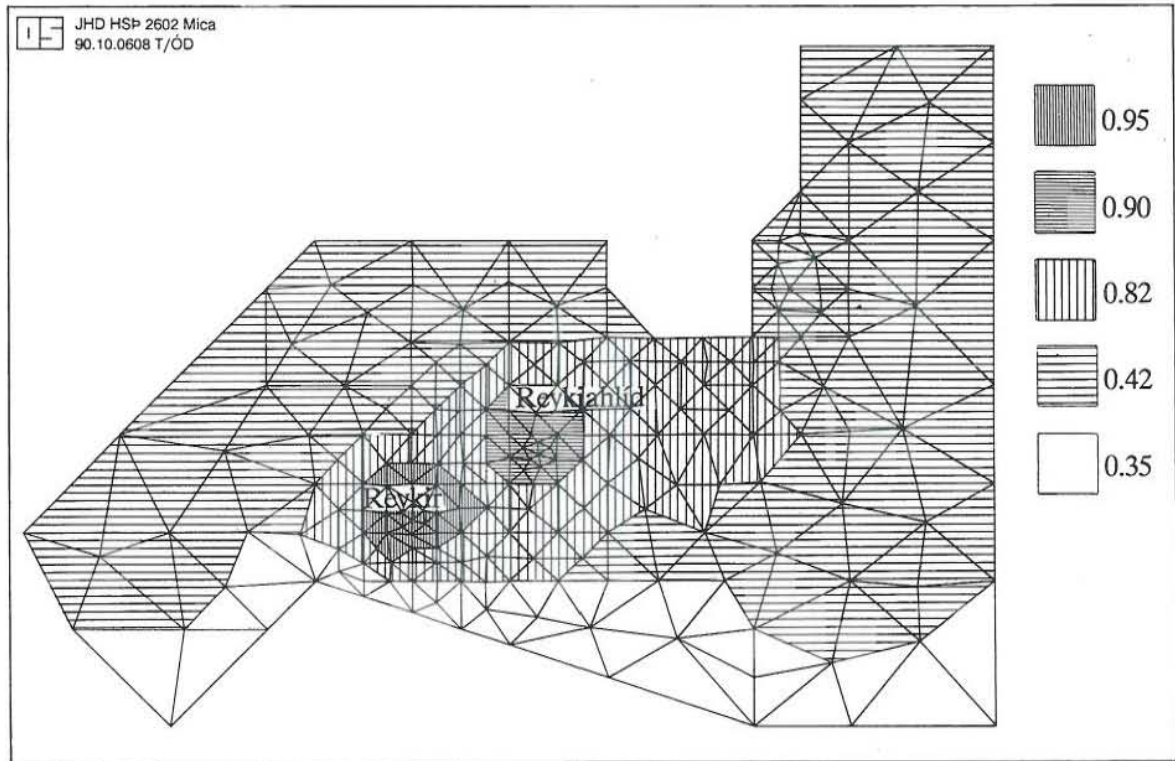
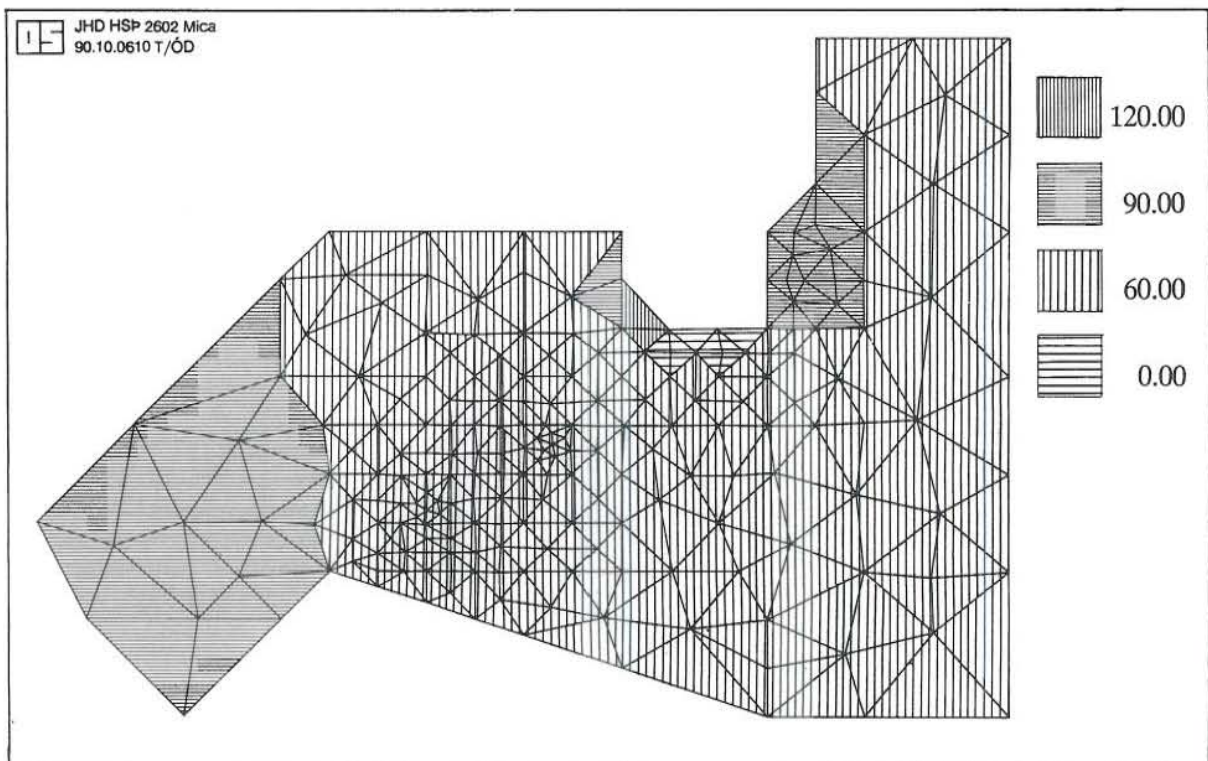


FIGURE 25: Map of anisotropy angles

FIGURE 26: Map of anisotropy $\text{SQRT } T_{yy}/T_{xx}$

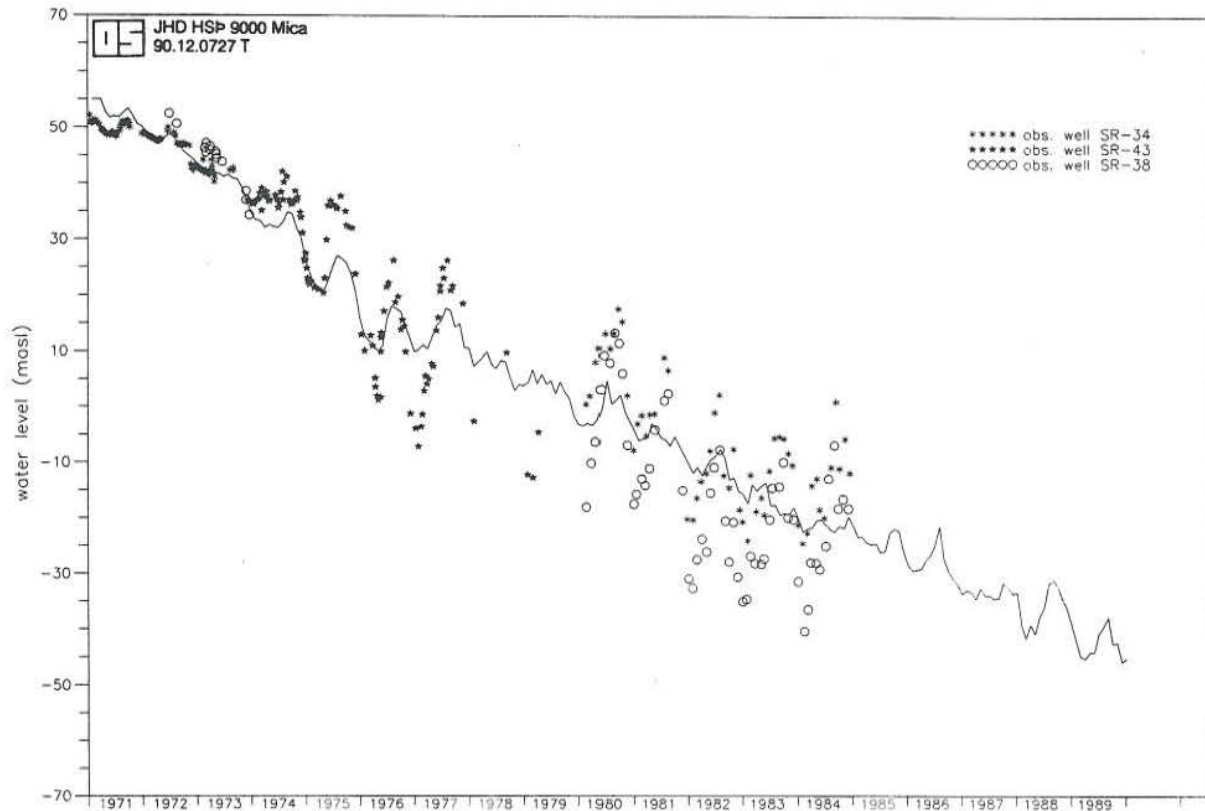


FIGURE 27: Measured and calculated drawdown, Reykir

4.4.3 Anisotropy

According to the previous assumptions mentioned in Section 4.3.3, anisotropy angles are established and shown in Figure 25. A map of the obtained values for transmissivity ratio $\sqrt{T_{yy}/T_{xx}}$ is shown in Figure 26. The initial value $\sqrt{T_{yy}/T_{xx}}$ was .35, but this value was shown to be very low, especially for the productive area. The obtained value from the model is near to 1 in the vicinity of the wells, and spreads along the anisotropy angle to the northeast.

4.4.4 Drawdown

Relatively poor fit is obtained with the model if measured and calculated drawdowns are compared, especially if fluctuations of the drawdown are taken into account. Figures 27, 28 and 29 show calculated and measured drawdowns for Reykir (SR 34,38 and 43), Reykjahlid (NR-15, MG-28), and Stardalur (S-1).

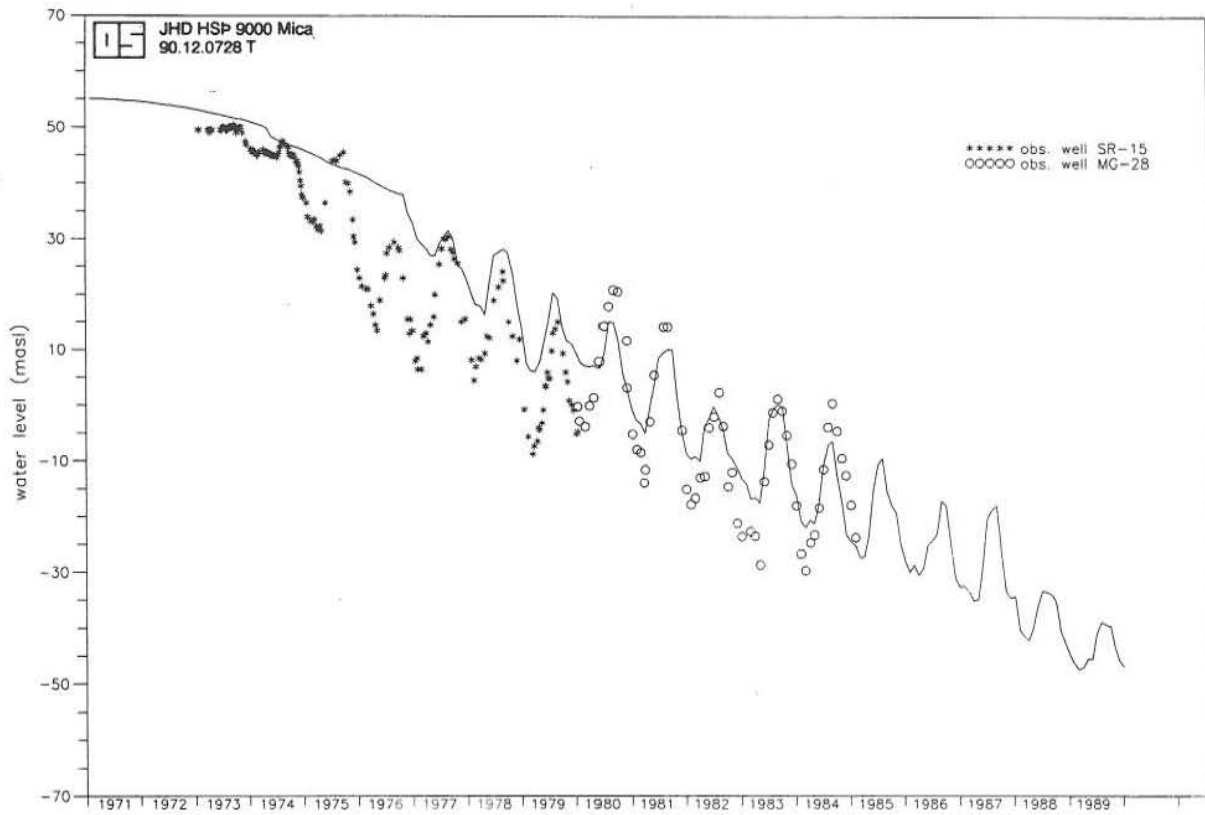


FIGURE 28: Measured and calculated drawdown, Reykjahlid

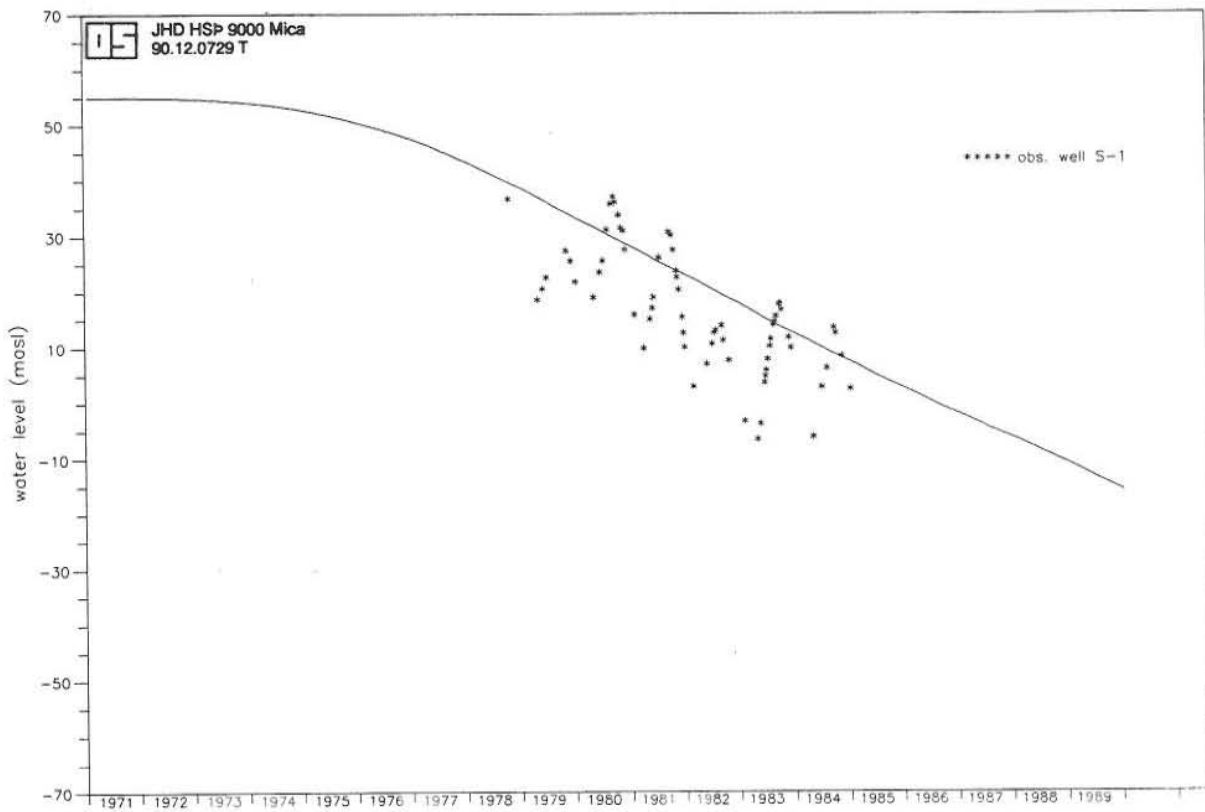


FIGURE 29: Measured and calculated drawdown, Stardalur

The model used is not able to produce the sharp changes in the drawdown. This is mainly due to the same disadvantages of the base assumptions used for establishing the primary conditions of the model and some disadvantages of the AQUA programme. One disadvantage is that production from the fields is simulated with only two wells. So, with this assumption, changes in production for single wells are covered with the average production from the field. For Reykir field especially, production on a monthly basis has small changes which cannot induce fluctuations in the drawdown. Another reason for small fluctuations of the drawdown is that the obtained value for the storage coefficient is very high and represents long-term behaviour of the reservoir, thus neglecting the short-term elastic change and fluctuation of the drawdown. If the average value and trend in the lowering of the drawdown is taken into account, then the model gives satisfactory fit between measured and calculated drawdown and could represent long-term behaviour of the productive areas.

After calibration, the model is used for calculations of the drawdown for the year 1990 and for future prediction of the drawdown for the year 2000. Results of the calculations are shown in Figures 30 and 31. The calculated drawdown for the year 1990 for productive areas is between 90 and 100 m, which is in the same range as values obtained by measurements.

For future prediction, the same average production as in year 1989 is assumed for the next 11 years (until year 2000). The obtained value for the drawdown in the productive areas will be between 130 and 140 m, with peaks of 145 m in the vicinity of the wells. This value is near to the value obtained by the lumped parameter model.

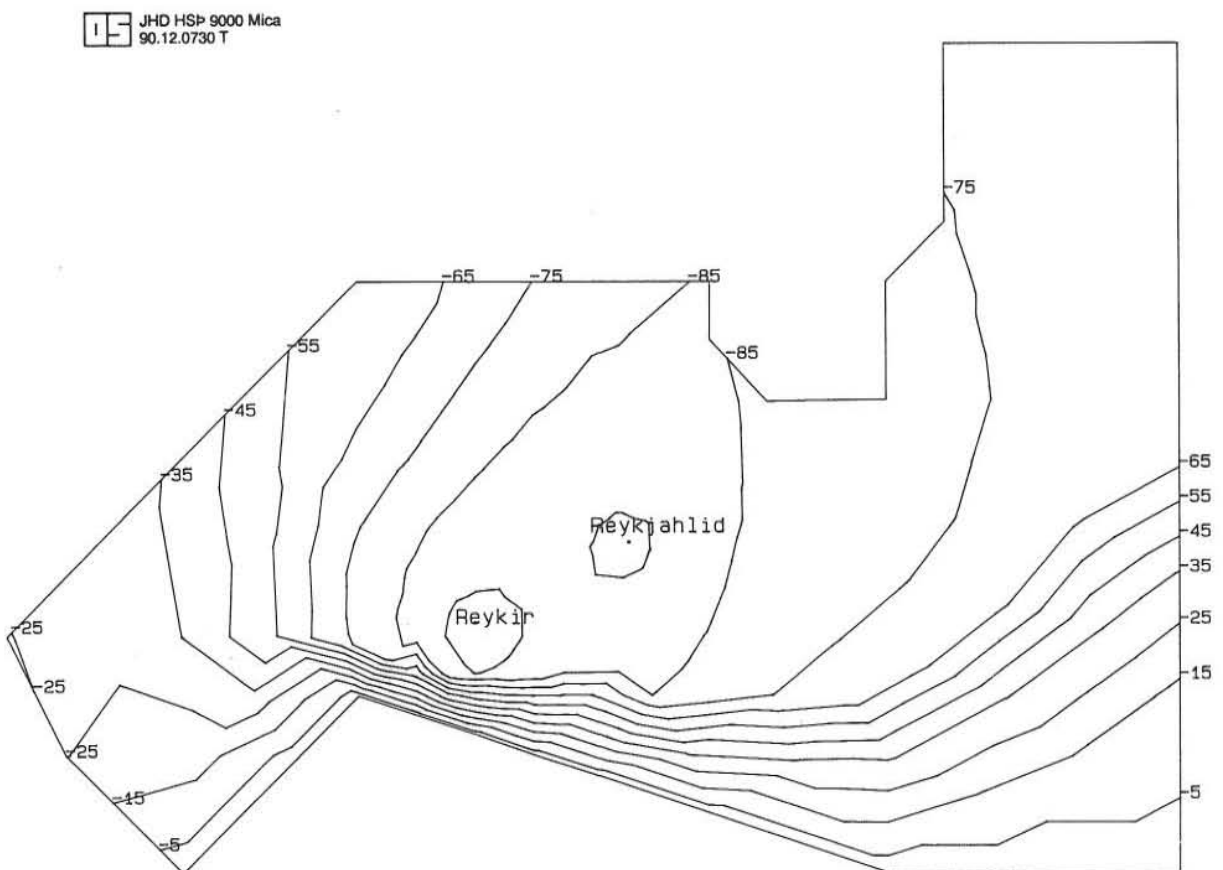


FIGURE 30: Calculated drawdown for Mosfellssveit geothermal field, year 1990

JHD HSP 9000 Mica
90.12.0731 T

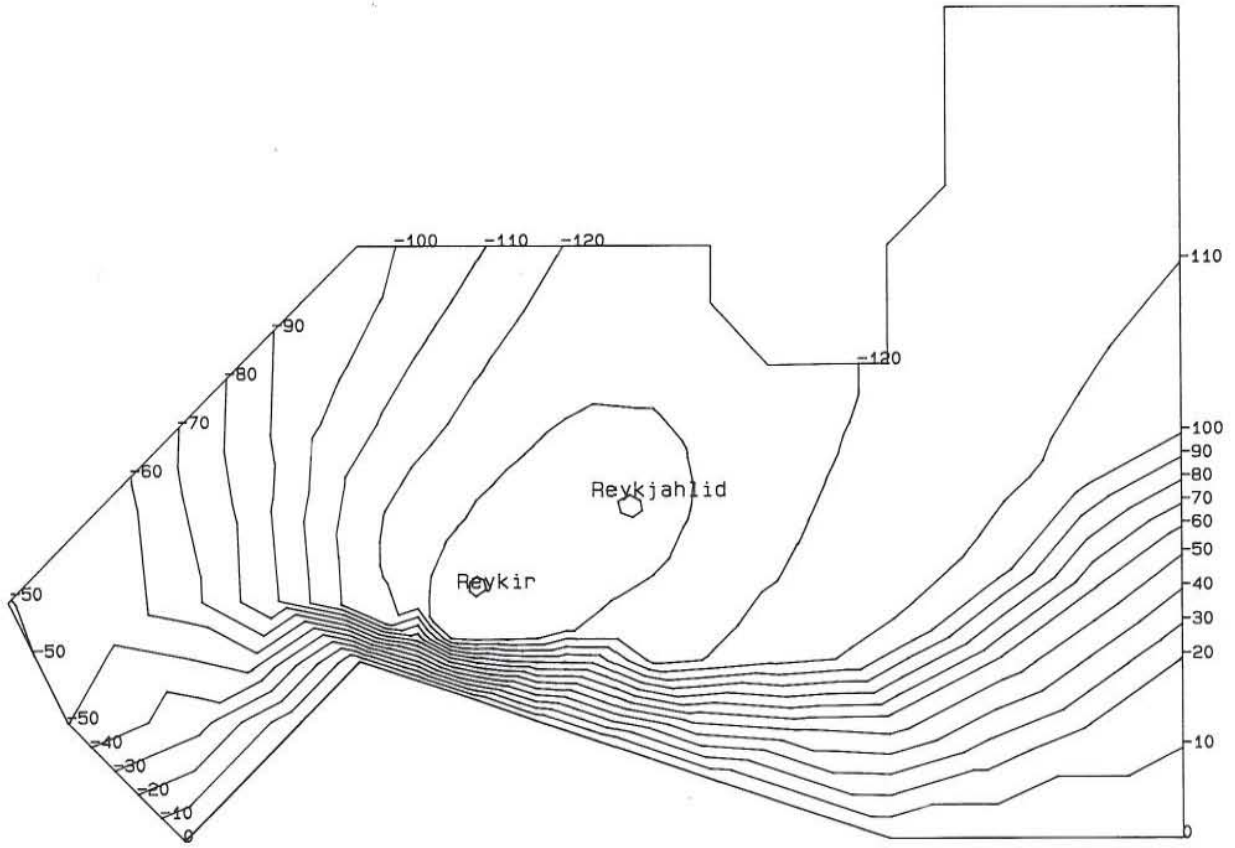


FIGURE 31: Calculated drawdown for Mosfellssveit geothermal field, year 2000

CONCLUSIONS AND RECOMMENDATIONS

In 1970 the free flow from the reservoir was 300 l/s and had reached relatively steady-state conditions, meaning that the natural recharge to the system was about the same as the amount withdrawn (Sigurdsson et al., 1985). The increase in production from 300 l/s in 1970 to 1200 l/s in 1989 has not induced recharge to the system to the same extent.

From the trend of the measured and calculated curves for the water level obtained from lumped and distributed groundwater flow models, it is quite obvious that with present production no steady-state conditions in the reservoir can be reached until year 2000. So, the recharge in the system is much less than production for the present drawdown.

Assuming production from the field for the next 11 years to be the same as in 1989, the drawdown will decline from 95 m in 1989 to 140 m in 2000, with the same tendency in the future.

It is possible to reach relatively steady-state conditions with an average production rate of 500 l/s per year, which is little more than half the production of 1989.

The geothermal reservoir shows two different storage mechanisms. At the start of production, the storage coefficient is controlled by the liquid/formation compressibility with characteristic values for the confined aquifers approximately $2.2 \cdot 10^{-4}$ (Thorsteinsson, 1975). In later production, the storage coefficient is controlled by the mobility of the free surface with a value of 0.1, which is near to the effective porosity.

A great amount of geological, geophysical, and geochemical data is available about the area where the geothermal field is situated, but the water level measurements cover only the field area, with the exception of observation well S-1 in Stardalur, which is 7 km to the northeast of the field. For more accurate numerical modelling of the field, it is necessary to cover areas outside the field with observations of water level and temperature measurements, in order to estimate a distribution of parameters which could be used for establishing a more accurate numerical model of the field.

AKNOWLEDGEMENTS

It gives me great pleasure to express my gratitude to Dr. Snorri Pall Kjaran for his excellent guidance during the training period and for critically evaluating the work presented in this report.

I would like to thank Dr. Ingvar B. Fridleifsson, the director of the UNU Geothermal Training Programme for providing excellent work conditions during my studies.

I would also like to thank Dr. Valgardur Stefansson for his excellent organization of well testing in Krafla, Josef Holmjarn for his guidance in the application and instrumentation of well logging methods, Ludvik S. Georgsson for his excellent lectures in geophysics and his guidance during the training course, and Marcia Kjartansson for carefully editing the material and for her technical preparation of the whole report.

Special thanks go to Dr. Mihailo Milivojevic, Mr. Mihajlo Simic and Prof. Javan Peric for their support during my six months' training course in Iceland.

NOMENCLATURE

- a_L - longitudinal dispersivity (m)
- a_T - transversal dispersivity (m)
- A_1 - surface area, upper aquifer (m^2)
- A_2 - surface area, lower aquifer (m^2)
- b_1 - thickness, upper aquifer (m)
- b_2 - thickness, lower aquifer (m)
- c - solute concentration (kg/m^3)
- c_0 - concentration of vertical inflow (kg/m^3)
- c_w - concentration of injected water (kg/m^3)
- C_1 - specific heat capacity of the liquid
- C_s - specific heat capacity of the porous media
- C_1 - constant (URF) (m)
- C_2 - constant (URF) (m)
- D_m - molecular diffusivity (m^2/s)
- D_{xx} - dispersion coefficient in x direction
- D_{yy} - dispersion coefficient in y direction
- E_i - enthalpy of the inlet water
- E_o - enthalpy of the outlet water
- h - groundwater head (m)
- h_0 - constant potential (m)
- h_1 - potential, upper aquifer (m)
- h_2 - potential, lower aquifer (m)
- K_1 - permeability, upper aquitard (m/s)
- K_2 - permeability, lower aquitard (m/s)
- K_d - distribution coefficient
- m_1 - thickness, upper aquitard (m)
- m_2 - thickness, lower aquitard (m)
- P_t - thermal power (MW)
- R - infiltration (m/year)
- R_d - retardation coefficient
- s - storage coefficient
- s_1 - drawdown upper, aquifer (m)
- s_2 - drawdown lower, aquifer (m)
- S_1 - storage coefficient, upper aquifer
- S_2 - storage coefficient, lower aquifer
- t - time (s)
- T - temperature ($^{\circ}C$)
- T_0 - temperature in vertical inflow ($^{\circ}C$)
- T_m - total mass (kg/s)
- TE_i - total enthalpy of the inlet water (KW)
- TE_o - total enthalpy of the outlet water (KW)
- T_{xx} - transmissivity in x direction (m^2/s)
- T_{yy} - transmissivity in y direction (m^2/s)
- Q - pumping/injection (m^3/s)
- Q_1 - pumping rate, upper aquifer (m^3/s)
- Q_2 - pumping rate, lower aquifer (m^3/s)
- V - velocity (m/s)
- v_f - specific volume (l/kg)

Greek symbols:

- β_1 - retardation coefficient
- β_2 - specific heat capacity coefficient
- γ_1 - parameter, ($K_1/m_1 * A_1$)
- γ_2 - parameter, ($K_2/m_2 * A_2$)
- λ_1 - decay constant, upper aquifer (s^{-1})
- λ_2 - decay constant, lower aquifer (s^{-1})
- ρ_l - density of the liquid (kg/m^3)
- ρ_s - density of the porous media (kg/m^3)
- ϕ - porosity

REFERENCES

- Axelsson, G., 1989: Simulation of pressure response data from geothermal reservoirs by lumped parameter models. 14th Workshop on geothermal reservoir engineering, Stanford, California, in press.
- Bodvarsson, G., 1987: Geothermal reservoir physics. UNU G.T.P., Iceland, report 2, 131 pp.
- Einarsson, T., 1954: A survey of gravity in Iceland. Soc. Scient. Islandica, 30, 22 pp.
- Fridleifsson, I. B., 1973: Petrology and structure of the Esja Quaternary volcanic region, southwest Iceland. Ph.D. Thesis, Oxford University, 208 pp.
- Fridleifsson, I.B., 1975: Lithology and structure of geothermal reservoir rocks in Iceland. Second UN symposium on the development and use of geothermal resources, San Francisco, Proceedings, 371-376.
- Kjaran, S. P., 1986: Geothermal reservoir engineering experience in Iceland. Nordic Hydrol. 17, 417-438.
- Palmason, G., Arnorsson, S., Fridleifsson, I.B., Kristmannsdottir, H., Saemundsson, K., Stefansson, V., Steingrimsson, B., Tomasson, J. and Kristjansson, L., 1978: The Iceland crust: Evidence from drillhole data on structure and processes. Am. Geophys. Union, Ewing series 2, 43-65.
- Sigurdsson, O., Kjaran, S. P., Thorsteinsson, Th., Stefansson, V. and Palmason, G., 1985: Experience of exploiting Icelandic geothermal reservoirs. International symposium on geothermal energy, Kailua-Kona, Hawaii, Proceedings, 357-373.
- Tomasson, J., Fridleifsson, I. B., and Stefansson, V., 1975: A hydrological model for the flow of thermal water in southwestern Iceland with special reference to the Reykir and Reykjavik thermal areas. Second UN symposium on the development and use of geothermal resources, San Francisco, Proceedings, 643-648.
- Thorsteinsson, Th., 1975: Redevelopment of the Reykir hydrothermal system in southwest Iceland. Second UN symposium on the development and use of geothermal resources, San Francisco, Proceedings, 2173-2180.
- Vatnaskil Consulting Engineers, 1989: AQUA user's manual. Vatnaskil, Reykjavik.
- Zhou Xi-Xiang., 1980: Interpretation of subsurface temperature measurements in the Mosfellssveit and Ölfusdalur geothermal areas, SW-Iceland. UNU G.T.P., Iceland, report 7, 101 pp.